

The *Chandra* view of NGC 1800 and the X-ray scaling properties of dwarf starbursts

J. Rasmussen^{1*}, I. R. Stevens², T. J. Ponman²

¹ Astronomical Observatory, University of Copenhagen, Juliane Maries Vej 30, DK-2100 Copenhagen Ø, Denmark

² School of Physics and Astronomy, University of Birmingham, Edgbaston, Birmingham B15 2TT, UK

arXiv:astro-ph/0407284v1 14 Jul 2004

ABSTRACT

The superb spatial resolution of *Chandra* is utilized to study the X-ray morphology of the dwarf starburst galaxy NGC 1800 embedded in a small group of galaxies. Diffuse galactic emission is detected, extending several kpc above the galactic plane, with an overall morphology similar to the galactic winds seen in nearby X-ray bright starburst galaxies. This makes NGC 1800 the most distant dwarf starburst with a clear detection of diffuse X-ray emission. The diffuse X-ray luminosity of $1.3 \pm 0.3 \times 10^{38}$ erg s⁻¹ accounts for at least 60 per cent of the total soft X-ray output of the galaxy. A hot gas temperature of $kT = 0.25$ keV and metallicity $Z \approx 0.05Z_{\odot}$ are derived, the latter in consistency with results from optical spectroscopy of the interstellar medium. Our failure to detect any hot gas associated with the embedding galaxy group translates into an upper limit to the group X-ray luminosity of $L_X < 10^{41}$ erg s⁻¹. There is no convincing evidence that the outflowing wind of NGC 1800 is currently interacting with any intragroup gas, and mechanical considerations indicate that the wind can escape the galaxy and its surrounding HI halo, eventually delivering energy and metals to the intragroup gas. Properties of NGC 1800 are compared to those of other dwarf starburst galaxies, and a first detailed discussion of the X-ray scaling properties of this population of objects is given, set against the equivalent results obtained for normal starburst galaxies. Results indicate that dwarf starbursts to a large degree behave as down-scaled versions of normal starburst galaxies.

Key words: ISM: jets and outflows – galaxies: individual: NGC 1800 – galaxies: starburst – galaxies: haloes – X-rays: galaxies.

1 INTRODUCTION

Starbursts, periods of short but intense star formation, and associated galactic winds, are recognized as key elements in the context of galaxy formation and evolution (e.g. Heckman, Armus & Miley 1990). Starburst winds also constitute a viable candidate for the preheating mechanism (Kaiser 1991; Evrard & Henry 1991), thought to be at least partly responsible for the observed entropy level in the intergalactic medium of groups and clusters of galaxies, a level which is poorly explained by models of structure formation invoking gravitational interactions alone (Ponman, Cannon & Navarro 1999).

Gas loss in galactic starburst winds is well-established, and can result in a significant fraction of the interstellar medium being removed (Read, Ponman & Strickland 1997; Strickland & Stevens 2000; Read & Ponman 2001).

Whilst a rapidly moving cluster galaxy may be ram-pressure stripped by its motion through the intracluster

medium (ICM), much of the starburst activity in denser environments is likely to take place in groups, where velocities are too low for stripping to be a very effective process (Gaetz, Salpeter & Shaviv 1987). Under these circumstances, the confining ICM might cause the wind to stall, and prevent gas escaping from the galaxy (Babul & Rees 1992; Murakami & Babul 1999). This would have substantial implications both for galaxy evolution (much reduced gas loss) and for the ICM (reduced metal enrichment and energy injection). Bearing in mind that most galaxies are found in groups (Tully 1987; Eke et al. 2004), that a substantial fraction of star formation is bursty (Heckman et al. 1998 and references therein), and that interactions in groups may actually trigger starburst activity (e.g. Zou et al. 1995), results of this process are of great importance for our understanding of galaxy evolution and the evolutionary relationship between group galaxies and their surroundings.

In the absence of a confining medium, simulations indicate that a superwind will break out into the interstellar medium (ISM), driving a shell of swept-up material which eventually fragments due to Rayleigh–Taylor instabilities

* E-mail: jr@astro.ku.dk

(Strickland & Stevens 2000). The resulting escape of both pristine and enriched gas from the galaxy would be especially dramatic for low-mass galaxies, due to their smaller escape velocities. However, if a hot and dense ICM is present, the wind is expected to grow more slowly, perhaps even stall, and the swept-up shell not to immediately fragment due to its higher density (Murakami & Babul 1999). This might leave a slowly cooling bubble of hot gas of significantly higher density n compared to a freely escaping wind (resulting in a higher wind X-ray luminosity, since $L_X \propto n^2$). In order to explain the metal abundance and extended star formation observed in many low-mass galaxies, some studies (e.g. Legrand et al. 2001) invoke the presence of extended gaseous galactic haloes, acting as a barrier to the escape of starburst winds. The validity of this explanation could be questioned for low-mass galaxies in groups, where such haloes, after all, might be stripped.

Models and hydrodynamical simulations have been used to investigate the effect of an ambient ICM on the properties of a galaxy wind (Murakami & Babul 1999; Silich & Tenorio-Tagle 2001), indicating that for sufficiently high ICM thermal pressures the ICM can indeed provide a confining mechanism. However, little effort has been invested in quantifying the conditions required for ICM confinement. Furthermore, since no X-ray observations have been reported of starburst galaxies embedded in the hot ICM of groups or clusters, apart from the very low density gas in the compact group HCG16 (Turner et al. 2001), such simulation results remain to be tested by direct observations.

Starburst winds may also be responsible for “preheating” the ICM in groups and clusters, most notably evidenced by the entropy profiles of hot gas in groups (e.g. Ponman et al. 1999; Sun et al. 2003; Ponman, Sanderson & Finoguenov 2003; Rasmussen & Ponman 2004), and they may even be capable of sweeping out a non-negligible fraction of the ICM from the most loosely bound systems (Davis, Mulchaey & Mushotzky 1999). Further, some combination of winds and stripping is expected to be responsible for the observed chemical enrichment of the ICM. There is some controversy, however, as to the ICM metallicity of groups, and very low values compared to those found in clusters have been reported (e.g. Davis et al. 1999). If true, this could imply that galactic winds in some cases are suppressed by environment, a possibility of potential relevance also to clusters, since groups act as cluster precursors in hierarchical structure formation scenarios. If gas loss from galaxies is suppressed in groups, the metals in the cluster ICM may have been put in place more recently than is often supposed.

In an attempt to shed light on these issues and clarify the role of the ICM in the late stages of a starburst wind, we obtained *Chandra* data of the dwarf starburst galaxy NGC 1800, located in galaxy group no. 62 in the catalog of Maia, da Costa & Latham (1989). NGC 1800 was selected on the basis of its proximity, its relatively small distance from the centre of the group in which it is embedded (referred to as MdCL62 in the following), and because it is well inclined to our line of sight, thus allowing an efficient identification of sources in the disc and a clear view of any hot gas expanding out of the galactic plane. The galaxy was detected in the *IRAS* Survey, showing 60 μm and 100 μm

fluxes of $S_{60} = 0.79$ Jy and $S_{100} = 1.75$ Jy, hence displaying a warm far-infrared (FIR) ‘temperature’ ($S_{60}/S_{100} = 0.45$), indicative of starburst activity. It is, indeed, recognized as a *bona fide* starburst (e.g. Calzetti et al. 1995). It further seemed a particularly attractive target for a study of this type, given that $\text{H}\alpha$ observations have revealed filamentary emission extending well above the disc midplane, consistent with the picture that hot gas is being funneled above the disc (Hunter 1996). In this case there may be evidence that the swept-up shells have not fragmented completely and that the $\text{H}\alpha$ emission marks the edge of a stalled or slowly moving wind. Additional motivation for studying NGC 1800 was provided by the fact that only a handful of active dwarf starbursts have been studied in detail in X-rays, so the generic X-ray properties of this class of objects remain poorly established. Furthermore, since dwarf galaxies are among the earliest objects to form (and produce stars) in hierarchical structure formation scenarios, the study of nearby dwarfs may provide clues to the importance of different processes acting during the earliest stages of structure formation in the Universe.

As is the case for many dwarf galaxies, the exact Hubble type of NGC 1800 is not well-determined. It is most likely a spiral (although it has been claimed to be irregular, see e.g. Hunter 1996), possibly containing a bar, and possibly of Magellanic type. Here we take it to be of SBm type, consistent with its stellar mass-to-light ratio of $M/L_B \approx 3$ (Gallagher, Hunter & Knapp 1981; typical of larger spirals but near the upper extreme of irregulars). The optical extent can be conveniently parameterized through D_{25} , the ellipse outlining a B -band isophotal level of 25 mag arcsec^{-2} . The galaxy group MdCL62, of which NGC 1800 is a member, contains five other galaxies, none of which are covered by this *Chandra* pointing. Some characteristics for the galaxy and the group are listed in Table 1.

Section 2 deals with details of the observation and analysis, Section 3 presents results for the X-ray emission of NGC 1800 and the embedding group, and in Section 4 we discuss the properties and possible fate of the NGC 1800 starburst wind. Section 5 compares NGC 1800 to other dwarf starbursts, and discusses the scaling properties of starburst galaxies down into the dwarf regime. Summary and conclusions are presented in Section 6. $H_0 = 75 \text{ km s}^{-1} \text{ Mpc}^{-1}$ is assumed throughout. The distance of NGC 1800 is then 7.4 Mpc (Tully 1988), and 1 arcmin corresponds to ~ 2.2 kpc.

2 OBSERVATION AND ANALYSIS

NGC 1800 was observed by *Chandra* (obs. ID 4062) with the ACIS-S3 chip as aimpoint, for an effective exposure time of 46.2 ks, and with the CCD’s at a temperature of -120° C . The presumed group centre was situated on the I2 chip. Data were telemetered in Very Faint mode which allows for superior background subtraction relative to standard Faint mode. To exploit this, the data were reprocessed and background screened using the `acis_process_events` tool in CIAO v2.21. Bad pixels were screened out using the bad pixel map provided by the pipeline, and remaining events were grade filtered, excluding ASCA grades 1, 5, and 7.

For the analysis of NGC 1800 we considered events on the S3 chip only. Periods of high background were filtered

Table 1. General properties of the NGC 1800 galaxy and the MdCL62 group. Absolute B magnitude and D_{25} (major and minor diameter) characteristics are mean data from the Lyon-Meudon Extragalactic Database (LEDA), θ_{D25} is the D_{25} major axis position angle north eastwards; inclination (the angle of the polar axis with respect to the line of sight) taken from the NASA/IPAC Extragalactic Database (NED); group velocity dispersion σ taken from the catalog of Maia et al. (1989) and dynamical mass M from Gallagher et al. (1981); projected distance R_{proj} between NGC 1800 and the group centre computed from the angular offset.

| Name | RA (J2000) | Dec (J2000) | Hubble type | M_B | D_{25} (arcmin) | θ_{D25} (deg) | Incl. (deg) |
|----------|---------------|----------------|-------------|--------|----------------------|-------------------------|----------------|
| NGC 1800 | 05 06 25.4 | -31 57 15 | SBm | -16.86 | (2.00, 1.15) | 106 | 64 |

| Name | RA (J2000) | Dec (J2000) | N_{gal} | σ (km s $^{-1}$) | M (M $_{\odot}$) | R_{proj} (kpc) |
|--------|---------------|----------------|-----------|-----------------------------|------------------------|---------------------|
| MdCL62 | 05 05 41.0 | -31 53 00 | 6 | 260 | 6×10^{13} | 20 |

using 3σ clipping of the 2.5–7 keV lightcurve extracted from this chip in 200 s bins, excluding bright point sources and a 2 arcmin diameter circle centred on the (optical) centre of the galaxy. The cleaning level resulting from this approach is potentially sensitive to the adopted bin size, since $\sigma \simeq (\text{counts bin}^{-1})^{1/2}$; we found, however, that the cleaned exposure time stayed constant to within 2 per cent for bin sizes 100–1000 s. Some flares in the resulting lightcurve are evident, and removing the affected periods leaves a total of 34.6 ks of useful exposure time.

Point sources were identified on S3 using the wavelet-based CIAO tool `wavdetect`, adopting a threshold significance of 1.8×10^{-6} , which should limit the number of spurious detections on the chip to ~ 1 . A total of 36 sources were detected, in fair agreement with the statistical expectation of ~ 25 background sources for a 35 ks pointing (cf. Summers et al. 2003). We also tried `vtpdetect` and `celldetect` with default settings, but both methods seem to miss the fainter point sources, so the `wavdetect` results were taken to be the most reliable. The detection run was repeated with lower thresholds to test if sources just below the adopted threshold were present; this was not found to be the case. A total of three point sources were detected inside D_{25} , with two more just outside, some of which may of course be unassociated with NGC 1800. Unless otherwise specified, all sources were masked out in all further analysis, using their 3σ detection ellipses from `wavdetect`.

Fig. 1 shows a raw soft-band image of the full S3 chip. It is immediately clear that very few source counts are present within the D_{25} ellipse. The other ellipse shown in the figure marks the region adopted for spectral extraction, hereafter denoted D_{spec} , centred at $(\alpha, \delta)_{2000} = (05^h 06^m 25\overset{s}{.}5, -31^\circ 57' 22.5'')$. Diffuse emission seems confined to this region, as will be demonstrated below. Rectangles labelled 'A', 'B', and 'C' in Fig. 1 represent the regions adopted for spectral background estimation. Using regions in the data themselves for this purpose rather than publicly available blank-sky fields seems preferable, given the small number of source counts, the limited extent of diffuse emission, and the potential contamination from group emission on the chip. Three partially overlapping regions, sized 5.5–9.3 arcmin 2 , were selected for background estimation, ensuring they were chosen neither too small, nor too

large, in order to limit sensibility to statistical errors and to suppress systematics resulting from any significant response variations across the chip. We found no statistically significant differences between the area-weighted mean count rates of the three background regions or in resulting best-fitting model parameters for background subtracted source spectra. Spectra were accumulated in bins containing at least 15 net counts and fitted assuming χ^2 statistics. All spectral results are presented for background region 'A'.

3 RESULTS

3.1 NGC 1800 diffuse emission

Images were produced in various energy bands with 1 arcsec pixels in order to search for diffuse emission in and around NGC 1800. To increase the signal-to-noise ratio (S/N) and highlight any such emission we employed a background reduction approach analogous to that of Fabian et al. (2003): Photons were removed if they had less than three neighbours inside a radius of 3 arcsec, resulting in a uniform and substantial reduction outside source regions across the chip. This method only served to enhance the contrast of source emission against the background, and the resulting images were used solely for display purposes and not for quantitative analyses such as the extraction of surface brightness profiles described below. Fig. 2 shows a background reduced 0.3–5 keV image of the central $\sim 3 \times 3$ arcmin 2 region around D_{25} , adaptively smoothed using the CIAO task `cssmooth`. Diffuse emission is clearly seen, along with four of the five point sources detected by `wavdetect` within or close to D_{25} (the faintest point source, labelled '2' close to the S edge of D_{25} and containing only four 0.3–5 keV counts, is not picked up by `cssmooth` in this case). The diffuse emission seems elongated in the northwest–southeast direction, confined inside an ellipse which is tilted at an angle of $\sim 45^\circ$ relative to the major axis defined by D_{25} . The emission extent is roughly 1.1×2.1 arcmin 2 (ellipse major axes), corresponding to an enclosed area inside D_{spec} of ~ 9 kpc 2 . To the north of the galaxy centre, the tip of the X-ray emission coincides with the central region of a web-like structure of H α –emission detected by Hunter (1996), the approximate position and extent of which is outlined by a dashed rectangle in the fig-

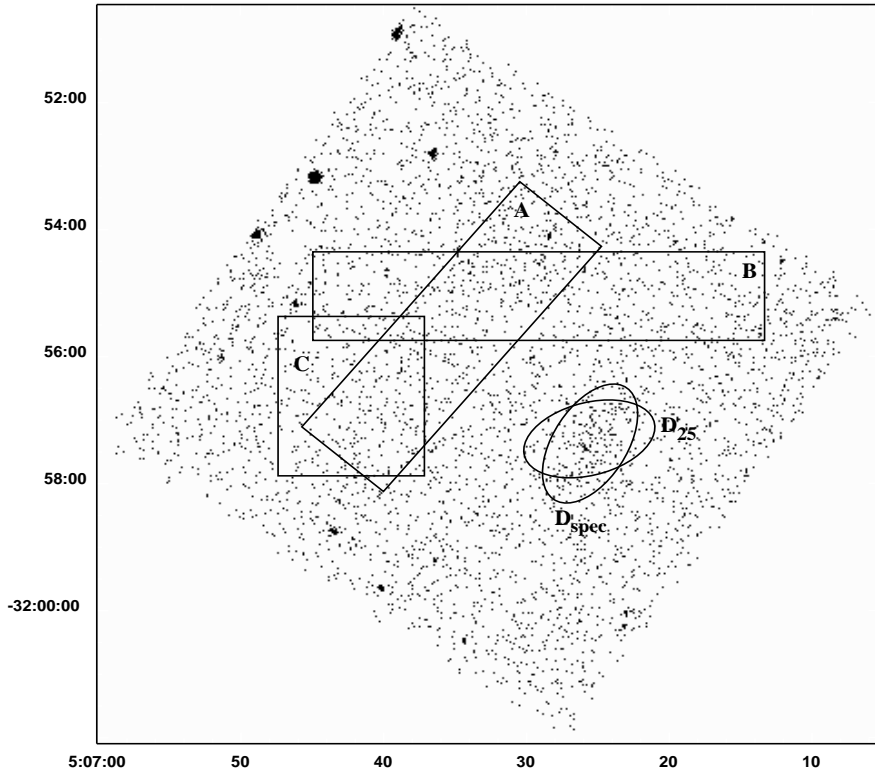


Figure 1. Raw 0.3–2 keV image (spatial scale $1.5 \text{ arcsec pixel}^{-1}$) showing the regions used for extraction of source spectra (D_{spec}), background spectra (rectangles), and the D_{25} ellipse determined from B -band isophotes. North is up and east is to the left.

ure. To the south, a $\text{H}\alpha$ shell was detected (marked as a dashed line), approximately where D_{25} intercepts the X-ray emission.

Inspection of images produced with larger binning revealed no evidence for low-surface brightness emission surrounding the source region. To investigate the surface brightness structure of the diffuse emission, we extracted the counts in a rectangular aperture with the same centre, position angle, and width as the D_{spec} ellipse of Figs. 1 and 2. The rectangle height was chosen such as to extend well beyond the D_{25} ellipse, in order to further test for the presence of diffuse emission outside D_{25} . The row-averaged profile is shown in Fig. 3, binned in 8 arcsec bins. The low number of counts precludes any firm conclusions regarding the shape of the profile, and thus the density distribution and 3-D morphology of the wind, but this figure clearly shows little evidence for diffuse emission outside D_{spec} where the profile is lost in the background. The lumps seen roughly 100 arcsec away at either side of the D_{spec} centre are not highly significant, and could not be associated with obvious features in the raw or smoothed images, or with detector artefacts when viewing the data in detector coordinates.

For the extraction of spectra of the diffuse emission we experimented with different apertures, finally adopting the D_{spec} region shown in Figs. 1 and 2 on the basis that it maximizes the S/N ratio while ensuring that nearly all source counts are included (increasing the size of the region does not increase the number of net counts, and extracting spectra e.g. inside D_{25} instead, yields ~ 30 per cent fewer net counts over roughly the same detector area). Spectra of the

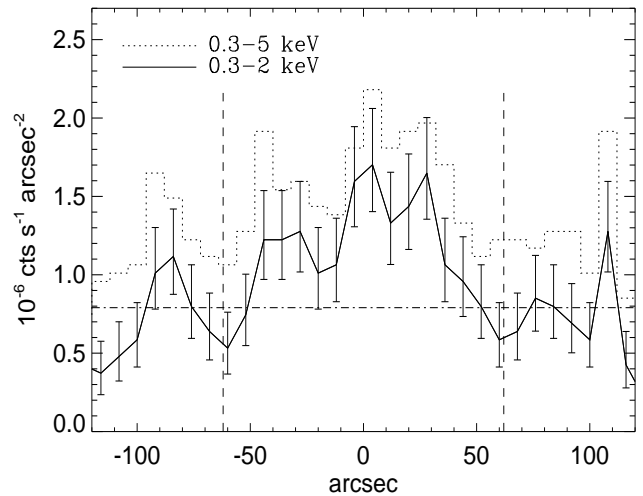


Figure 3. Surface brightness profiles of diffuse emission in a rectangular region centred on the D_{spec} ellipse, the extent of which (major axis) is shown by vertical dashed lines. 1σ error bars shown for the 0.3–2 keV profile have been calculated using the expressions of Gehrels (1986) for small-number Poissonian errors. Horizontal dash-dotted line marks the 0.3–2 keV background level as estimated from region 'A' in Fig. 1. The northern side of the galaxy is to the right.

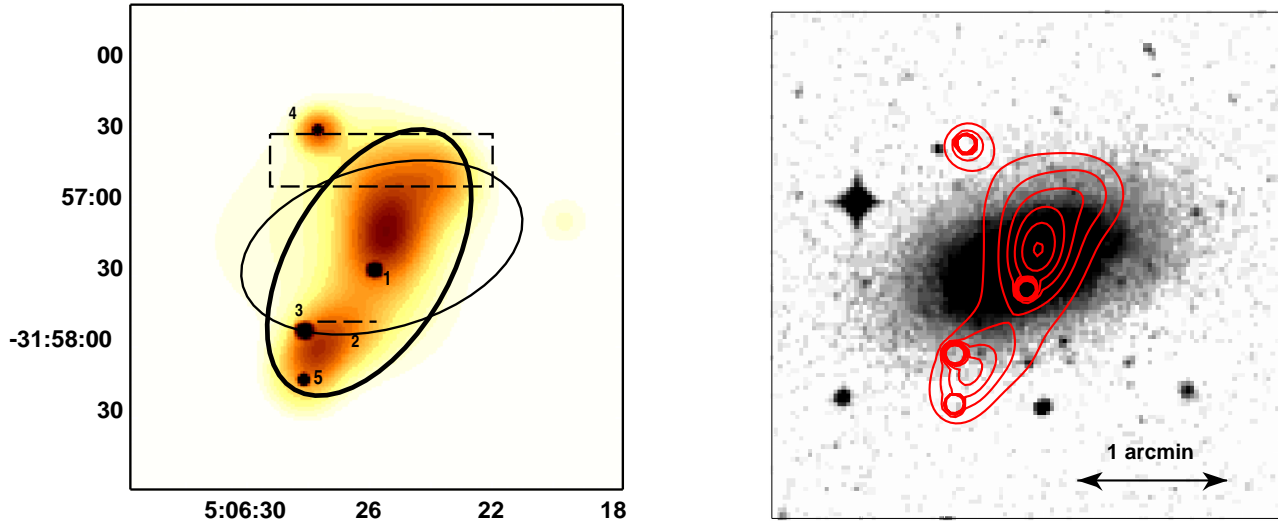


Figure 2. *Left:* Background reduced and adaptively smoothed 0.3–5 keV image ($3\sigma - 5\sigma$ significance range) displaying the central region around NGC 1800. Ellipses mark the same regions as in Fig. 1. Dashed box and line mark the H α features detected by Hunter (1996), see text. Numbers indicate the five point sources listed in Table 3 below. *Right:* Adaptively smoothed X-ray contours of the left figure overlayed on a Digitized Sky Survey optical image of NGC 1800.

diffuse emission were first extracted inside D_{spec} using responses weighted by the observed number of counts in the 0.3–3 keV band. The ACISABS model¹ was applied to the effective area file prior to spectral fitting, to account for the low-energy degradation in quantum efficiency of the ACIS chips. Only ~ 110 net counts from diffuse emission were detected inside D_{spec} . A good fit to the spectrum could nevertheless be obtained using an absorbed MEKAL model (reduced $\chi^2 = 0.84$) in XSPEC v11.3, whereas an absorbed power-law provided a poorer description (reduced $\chi^2 = 1.7$).

Preferably, responses should be weighted using the *incident* photon spectral distribution rather than the observed one (since the net effective area varies significantly with energy in the 0.3–3 keV range). Our best guess for the incident spectrum is the above best-fitting model, so spectra were re-extracted with this model acting as spectral weights. This, however, produced negligible differences with respect to the first result. The resulting spectrum is shown in Fig. 4. An absorbed MEKAL model was re-fitted to the spectrum. Given the small number of source counts and the ACIS low-energy calibration uncertainties, we chose to fix the absorbing column density N_H at the Galactic value of $1.54 \times 10^{20} \text{ cm}^{-2}$ (with which it was indeed found to be consistent), while Z was initially fixed at $0.5Z_\odot$, assuming solar abundances from Anders & Grevesse (1989). An absorbed power-law was also fitted, and Table 2 lists the results of spectral fitting. A differential emission measure model (CEMEKL in XSPEC) failed by a large margin to reproduce the flat spectral shape between 0.5 and 1 keV and is not included in the Table.

As can be seen from Table 2, a thermal MEKAL model provides a good fit, whereas a power-law is not a good description of the data. The low number of counts does not

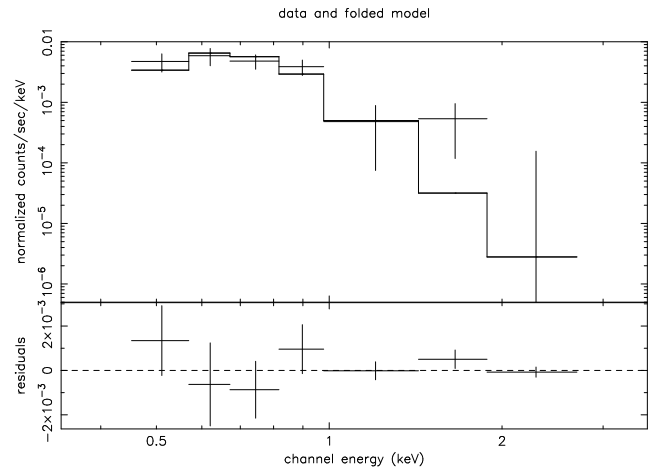


Figure 4. 0.3–3 keV spectrum of NGC 1800 diffuse emission, and best-fitting MEKAL plasma model. Bottom plot shows fit residuals.

warrant the introduction of additional model components for spectral fitting, so whether a second thermal component with $T \sim 0.6 - 0.8$ keV is present as in certain other dwarf starbursts (e.g. Summers et al. 2003; Summers et al. 2004; Hartwell et al. 2004) cannot be addressed with the present data.

The metal abundance, when left as a free parameter in the fits, is not well constrained. It is consistent with the (low) values of $Z_{\text{Fe}} \approx 0.05Z_\odot$ found for the Fe abundance of the soft thermal component in the starburst winds of NGC 253 and M82 (Ptak et al. 1997), and with results from optical spectroscopy of the three metal-deficient ($Z \approx 0.02Z_\odot$) star-forming blue compact dwarfs studied by Thuan et al. (2004). It also marginally agrees with estimates of the oxygen abundance in the ionized ISM of NGC 1800, $0.2Z_\odot <$

¹ Available from the CIAO web pages published by the *Chandra* X-ray Center, <http://cxc.harvard.edu/ciao/>

Table 2. Summary of spectral fits to the 0.3–3 keV diffuse emission. All errors are 1σ .

| Model | Fit results | Goodness of fit |
|---------------|---|---------------------------|
| ABS(MEKAL) | $T = 0.24^{+0.03}_{-0.02}$, $Z = 0.5Z_{\odot}$ (fixed) | $\chi^2 = 4.2/5 (= 0.84)$ |
| ABS(MEKAL) | $T = 0.26^{+0.05}_{-0.03}$, $Z = 0.05^{+0.22}_{-0.04} Z_{\odot}$ | $\chi^2 = 3.1/4 (= 0.77)$ |
| ABS(POWERLAW) | $\Gamma = 3.78^{+0.44}_{-0.40}$ | $\chi^2 = 8.7/5 (= 1.73)$ |

$Z_{\odot} < 0.4Z_{\odot}$ (Gallagher et al. 1981), and with X-ray results for the winds in the dwarf starbursts NGC 1569 ($> 0.25Z_{\odot}$; Martin, Kobulnicky & Heckman 2002), NGC 4449 ($0.32 \pm 0.08Z_{\odot}$; Summers et al. 2003), and NGC 5253 ($0.14 \pm 0.01Z_{\odot}$; Summers et al. 2004). While the metallicity of the ISM in dwarf galaxies as inferred from optical spectroscopy is usually agreed to be fairly low ($\lesssim 0.2$ – $0.3 Z_{\odot}$), there is a controversy as to the amount of chemical enrichment of any outflowing gas in these galaxies (see e.g. Tosi 2004). The picture suggested by the above observations is that dwarf starburst winds are not substantially enriched but may have metallicities comparable to the ISM. This is in line with some analytical models for the chemical evolution of dwarf galaxies (e.g. Larsen, Sommer-Larsen & Pagel 2001) and with the idea that the expanding shells sweep up a significant portion of the surrounding ISM material. In fact, hydrodynamical simulations (Strickland & Stevens 2000) suggest that wind abundance determinations from X-ray spectroscopy may reflect the values in disc and halo ISM to a substantial degree, but also that X-ray observations do not directly probe the global metallicity of winds. Furthermore, such simulations indicate the presence of a complex multi-phase environment with gas at a range of temperatures, and there is a well-known bias towards low derived abundances when a multi-temperature gas is fitted with a single-temperature model (Buote 2000; Buote et al. 2003). Consequently, the above results should be interpreted with some caution.

From the best-fitting model, with Z fixed at its best-fitting value of $0.05Z_{\odot}$, the resulting unabsorbed 0.3–3 keV flux from diffuse emission is $1.9 \pm 0.5 \times 10^{-14}$ erg cm $^{-2}$ s $^{-1}$, with errors from the fractional 1σ errors on the spectral normalization. At the distance of NGC 1800, this translates into a total diffuse luminosity of $1.3 \pm 0.3 \times 10^{38}$ erg s $^{-1}$.

The number of source counts from the five point sources detected within or close to D_{25} totals less than 90 (0.3–5 keV), so any detailed investigation of point source X-ray properties is excluded. A power-law fit to their combined spectrum suggests a photon index of $\Gamma \approx 0.8$ and a combined 0.3–3 keV flux of $1.2 \pm 0.2 \times 10^{-14}$ erg cm $^{-2}$ s $^{-1}$. Assuming the sources to be at the distance of NGC 1800, this would imply a combined 0.3–3 keV luminosity of $\approx 8 \times 10^{37}$ erg s $^{-1}$. Resolved point sources thus account for ~ 40 per cent of the observed soft X-ray emission, a value bracketed by the corresponding results for other dwarf starbursts (e.g. Ott, Martin & Walter 2003; Summers et al. 2003). These results are dominated by the two point sources outside D_{25} , however. The hardness of the best-fitting spectrum may suggest that these sources are intrinsically absorbed active galactic nuclei (AGN) and therefore are unassociated with

NGC 1800. Fitting these two sources alone produces a Γ of ~ 0.6 . Table 3 lists some properties of the five point sources. As can be seen from Fig. 2, none of these X-ray point sources have a bright optical counterpart, and it is not possible to associate them with near-infrared point sources or quasars detected in the 2 Micron All Sky Survey (2MASS). The inferred luminosities are representative of X-ray binaries, and we find no evidence for the presence of ultraluminous X-ray sources, with $L_X \sim 10^{39} - 10^{41}$ erg s $^{-1}$.

3.2 A hot gaseous halo around NGC 1800?

There is clear evidence from HI observations for gas extending well beyond the optical extent of the galaxy (out to twice the Holmberg radius $D_{26.5}$; Hunter, van Woerden & Gallagher 1994), and the presence of a diffuse H α halo has been claimed by Hunter (1996). Numerical simulations of disc galaxy formation (e.g. Toft et al. 2002) further predict the presence of a hot, X-ray emitting gaseous halo surrounding such galaxies. NGC 1800 is not a normal spiral, and, being possibly irregular, it might not even qualify as a disc galaxy. But a hot X-ray halo, fueled by outflowing bubbles of gas, could also be expected on the basis of the starburst activity in NGC 1800. To test for the presence of an X-ray emitting halo around the galaxy, a spectrum was extracted in an elliptic, 1.5 arcmin wide annulus outside the combined region of D_{25} and D_{spec} . We found no evidence for excess emission above the background in this annulus. The predictions of Toft et al. (2002), when extrapolated to a disc circular velocity of $V_c \approx 30$ km s $^{-1}$ as is relevant for NGC 1800 (Section 4.3), would suggest $T \lesssim 0.1$ keV and a 0.3–3 keV luminosity of $\sim 10^{37}$ erg s $^{-1}$ for the halo gas. For a $T = 0.1$ keV $Z = 0.3Z_{\odot}$ MEKAL plasma, the absence of a detection inside the adopted annulus translates into a 3σ upper limit on the 0.3–3 keV flux and luminosity of 6.6×10^{-15} erg cm $^{-2}$ s $^{-1}$ and 4.2×10^{37} erg s $^{-1}$, respectively, in consistency with the above expectations.

A trivial reason for the lack of a hot halo detection is that such a halo is simply too X-ray faint to be detectable in these observations. This is surely a realistic possibility, given the predictions of hot halo X-ray properties reported by Toft et al. (2002) and the observational results of Benson et al. (2000). Alternatively, the standard picture of disc galaxies surrounded by a quasi-hydrostatic halo containing gas at the virial temperature is invalid for low-mass systems and/or systems formed at high redshifts (see e.g. Birnboim & Dekel 2003). Dwarf galaxies satisfy both these criteria. The possibility also exists that any hot halo has been ram-pressure stripped through interactions with the group ICM (cf. Marcolini, Brighenti & D'Ercole 2003).

Table 3. Properties of the five point sources detected within or very close to the D_{25} ellipse, numbered according to increasing projected distance from the D_{25} centre (cf. Fig. 2). Background-subtracted count rates and luminosities are given in the 0.3–5 keV band, the latter values assuming a power-law spectrum of $\Gamma = 0.8$ from a fit to the combined spectrum. All errors are 1σ .

| Source no. | RA (J2000) | Dec (J2000) | Count rate (counts s $^{-1}$) | L_X (10 37 erg s $^{-1}$) |
|------------|---------------|----------------|-----------------------------------|--------------------------------------|
| 1 | 05 06 25.85 | −31 57 27.7 | $3.3 \pm 1.0 \times 10^{-4}$ | 1.9 ± 0.6 |
| 2 | 05 06 26.95 | −31 57 52.7 | $1.3 \pm 0.6 \times 10^{-4}$ | 0.7 ± 0.3 |
| 3 | 05 06 28.12 | −31 57 52.8 | $3.6 \pm 1.0 \times 10^{-4}$ | 2.0 ± 0.6 |
| 4 | 05 06 27.74 | −31 56 28.7 | $14.2 \pm 0.2 \times 10^{-4}$ | 7.9 ± 1.2 |
| 5 | 05 06 28.17 | −31 58 13.3 | $7.2 \pm 1.5 \times 10^{-4}$ | 4.0 ± 0.8 |

The presence of an extended HI halo, as demonstrated by Hunter et al. (1994), suggests, however, that ram pressure effects are not significant.

3.3 Group diffuse emission

The group centre in the Maia et al. (1989) catalogue (Table 1) is located on the I2 chip, but given that the group is rather sparse, the centre of the group potential may not be well-determined from optical observations. To give an appreciation of the nature of the group and the angular scales involved, we show in Fig. 5 the sky position of the optically determined group centre and the six member galaxies. There is no clear indication of the position of the group centre in the present X-ray data, so in order to search for X-ray emission from intragroup gas, we decided to extract large-area spectra of source-free regions on both the I2 and S3 chips. For background estimation, we employed the ‘period D’ blank-sky data of M. Markevitch², screened and filtered as for our data and taking advantage of the fact that the blank-sky data were also made in Very Faint mode. The σ – T relation of Helsdon & Ponman (2000) would suggest $T \approx 0.7$ keV for the intragroup gas, so any group X-ray emission is likely to be fairly soft. Differences in local soft X-ray background between source and background data could thus potentially influence the results. We therefore checked the exposure-weighted mean value of *ROSAT* All-Sky Survey soft (R45 band, ~ 0.5 – 0.9 keV) count rates in the two data sets, finding $1.01 \pm 0.10 \times 10^{-4}$ (for a 2×2 deg 2 region around NGC 1800) and $1.13 \pm 0.11 \times 10^{-4}$ cts s $^{-1}$ arcmin $^{-2}$ for source and background data, respectively, and hence no significant difference.

For the I2 chip, we performed a 3σ clipping of the data based on the 0.3–12 keV lightcurve, and excluded, from source and background data, the source regions found by `wavdetect` in source data. The blank-sky data were subsequently coordinate transformed to match the pointing characteristics of our source data, ensuring that source and background spectra could be extracted from identical detector regions. It was then confirmed for the S3 chip that the blank-sky background did not differ significantly from our local background estimates, by extracting a source and background spectrum inside D_{spec} and performing a fitting procedure analogous to that described in Section 3.1. Results

were in excellent agreement with those obtained using local background determinations (rectangles ‘A’–‘C’ in Fig. 1), including the resulting number of net counts inside D_{spec} . This in itself suggests that there is little group emission from gas along our line of sight to NGC 1800.

To search for group diffuse emission well outside D_{25} , a ‘full-chip’ spectrum was extracted, avoiding chip edges and excluding sources from `wavdetect` and the region covered by twice the ellipse axes of D_{25} (equivalent to the Holmberg radius of the galaxy, cf. Hunter et al. 1994). Within the 1σ background noise we found no evidence for excess emission in the 0.3–5 keV band on S3. The exercise was repeated for the I2 data, with the same result.

The MdCL62 group was not detected in the *ROSAT* All-Sky Survey, which features an exposure time of ≈ 500 s at this sky position. The L_X – σ relation of Helsdon & Ponman (2000), based on *ROSAT* data of 24 X-ray bright groups, would suggest a (bolometric) luminosity of $L_X \approx 1.5 \times 10^{42}$ erg s $^{-1}$. Assuming the emission to be uniformly distributed within 300 kpc (typical of the group radii probed by *ROSAT*), centred on the optical group centre, with $T = 0.7$ keV, $Z = 0.2Z_\odot$, and subject to the relevant value of N_H , a PIMMS calculation suggests that we should expect ~ 1300 and ~ 1800 counts on the I2 and S3 chips, respectively (0.3–5 keV, corrected for removed area). Although not corrected for vignetting, these estimates should be lower limits, as the true X-ray surface brightness distribution is expected to peak close to the observed region and thus should be well above the average value inside ~ 300 kpc on either chip. Even if the X-ray group centre is located 300 kpc away from the nominal aimpoint of this observation, with a surface brightness distribution following a standard β -model of $\beta = 0.5$ and $r_c = 100$ kpc (based on $r_{500} \approx 600$ kpc from its dynamical mass of $6 \times 10^{13} M_\odot$, cf. Table 1, and $r_c \sim 0.15r_{500}$ from Sanderson et al. 2003), the above estimates are still more than an order of magnitude above the observed values. It therefore seems safe to assume that $L_X < 10^{41}$ erg s $^{-1}$ for the intragroup gas, implying that the group is rather X-ray faint. This result is perhaps not surprising, given that all six group members are spirals or dwarf spirals, with the brightest member being the Scd spiral NGC 1679 at $M_B = -18.89$. In contrast, the dominant galaxy in X-ray bright groups is almost always of early-type (e.g. Mulchaey et al. 2003). The result also implies that the group falls well below the nominal L_X – σ relation of Helsdon & Ponman (2000). This relation is subject to a good deal of scatter, though, so it would seem premature

² <http://hea-www.harvard.edu/~maxim/axaf/acisbg/>

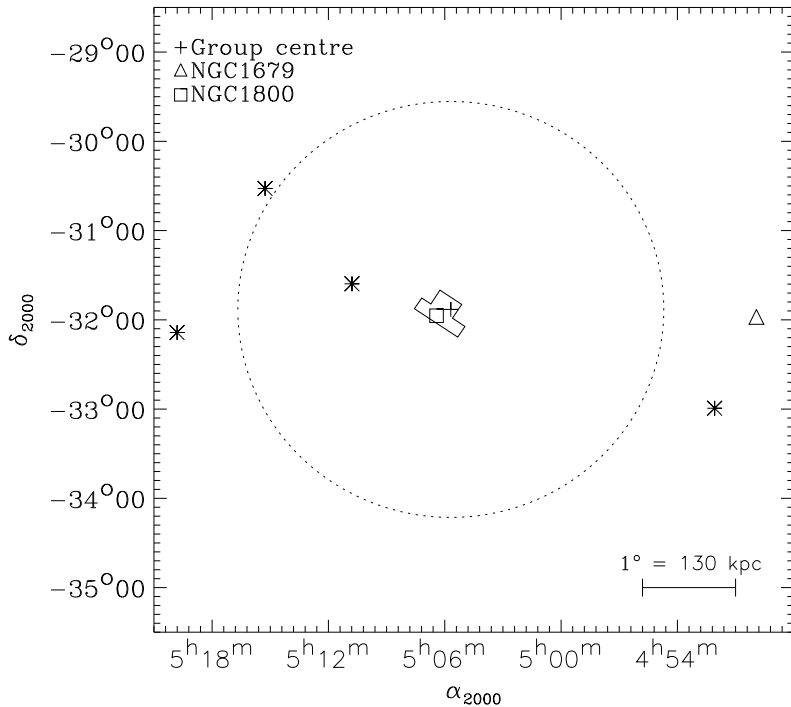


Figure 5. Galaxy distribution in the MdCL62 group in a $7 \times 7 \text{ deg}^2$ region. A cross marks the optically determined group centre, NGC 1800 is shown by a square, and the brightest group galaxy, NGC 1679, by a triangle. Remaining galaxies are represented by asterisks. Also outlined is the area covered by the ACIS CCD's (solid) for this observation, and the radius $r = 300 \text{ kpc}$ (dotted) used for estimating the X-ray luminosity of intragroup gas (see text).

to conclude, on these grounds, that σ for the group might be artificially boosted by the inclusion of galaxies unrelated to the group. The galaxy configuration suggests the group is somewhat unrelaxed, so perhaps the group is still only approaching a state of sufficiently high density to produce significant X-ray emission.

4 DISCUSSION

4.1 Hot gas and star formation properties

The X-ray luminosity and overall morphology of the hot X-ray gas in NGC 1800 is similar to that inferred for other nearby dwarf starburst galaxies, in which a hot, outflowing galactic wind has been detected. It is therefore natural to assume that the diffuse X-ray emission in NGC 1800 is the signature of such a wind. Using the derived gas parameters for NGC 1800 one can assess the physical properties of the X-ray emitting gas, once the size of the X-ray emitting volume has been estimated. Fig. 2 clearly suggests that this volume is nonspherical, so here it is assumed that the gas is confined inside an ellipsoid with two of the axes equal to those of D_{spec} and the third (the one along our line of sight) equal to the D_{spec} minor axis; this yields a total volume $V \approx 4.2 \times 10^{65} \text{ cm}^3$, of which only some fraction η is occupied by X-ray gas. From the spectral normalization A in XSPEC,

$$A = \frac{10^{-14}}{4\pi D^2} \int n_e n_H \, dV, \quad (1)$$

where D is the distance (Section 1), one can derive the fitted emission measure $EM \equiv \int n_e n_H \, dV \approx \eta n_e^2 V$, and hence the mean electron density $n_e \approx (EM/V\eta)^{1/2}$. This can then be combined with kT (Table 2) and L_X to infer the gas mass $M_{gas} \approx m_p n_e V \eta^{1/2}$, thermal pressure $P \approx 2n_e kT \eta^{-1/2}$, thermal energy $E_{th} \approx 3n_e kTV \eta^{1/2}$, cooling function $\Lambda = L_X/EM$, cooling time $t_{cool} \approx 3kT \eta^{1/2}/(\Lambda n_e)$, mass deposition rate $\dot{M}_{cool} = M_{gas}/t_{cool}$, and the mean particle velocity $\langle v_p \rangle = (2E_{th}/M_{gas})^{1/2}$. Most of these quantities are listed in Table 4. Unless otherwise stated, we will in the following take $\eta = 1$ for simplicity, and, where relevant, discuss the implications of this assumption.

The resulting mass of X-ray gas is well below the total neutral gas mass of NGC 1800 of $\sim 2 \times 10^8 \text{ M}_{\odot}$, as inferred from H α observations (Gallagher et al. 1981; corrected to our assumed distance), and an order of magnitude lower than the mass of ionized gas in the H α web north of the galaxy ($\sim 4 \times 10^7 \text{ M}_{\odot}$; Hunter 1996). The mass and thermal energy content of X-ray gas is also smaller than typical values inferred for non-dwarf starburst galaxies by similar methods (Read & Ponman 2001), but is comparable to published values for other dwarf starbursts (Martin et al. 2002; Ott et al. 2003; Summers et al. 2003, 2004; Hartwell et al. 2004). The thermal pressure in the wind corresponds to $P/k \sim 7 \times 10^4 \text{ K cm}^{-3}$, an order of magnitude larger than the ISM pressure in the Galactic midplane (Wolfire et al. 1995). We should mention, though, that results from hydrodynamical simulations (Strickland & Stevens 2000) indicate that only a small fraction of the total energy and mass content of winds is

Table 4. Physical properties of the hot X-ray gas in NGC 1800. See text for the dependence of each quantity on the volume filling factor η .

| n_e (cm $^{-3}$) | M_{gas} (M $_{\odot}$) | P (dyn cm $^{-2}$) | E_{th} (erg) | t_{cool} (Myr) | \dot{M}_{cool} (M $_{\odot}$ yr $^{-1}$) | $\langle v_p \rangle$ (km s $^{-1}$) |
|------------------------|-------------------------------------|--------------------------|--------------------------|----------------------------|---|--|
| 0.012 | 4.1×10^6 | 9.9×10^{-12} | 6.1×10^{54} | 1500 | 0.003 | 290 |

probed by observations of their soft X-ray emission, with most of the thermal and kinetic energy being carried by hot and rarefied low-emissivity gas which is difficult to detect observationally. Nevertheless, the above values provide a first handle on the wind properties of NGC 1800, and will enable a more detailed comparison to other starburst galaxies for which these quantities have been estimated using identical techniques (see Section 5).

The global star formation rate (SFR) of NGC 1800 can be estimated from the total H α luminosity of the galaxy. For $L(\text{H}\alpha) \approx 4 \times 10^{39}$ erg s $^{-1}$ (Hunter 1996; corrected to the assumed distance), the relation of Kennicutt, Tamblyn & Congdon (1994), $\text{SFR}(\text{M}_\odot \text{ yr}^{-1}) = L(\text{H}\alpha)/(1.26 \times 10^{41} \text{ erg s}^{-1})$, would suggest an SFR of $\approx 0.03 \text{ M}_\odot \text{ yr}^{-1}$. For the adopted distance, this agrees well with earlier estimates by Gallagher et al. (1981) and Hunter et al. (1994), also based on H α emission fluxes. The star formation rate can also be estimated from the (far)-infrared luminosity L_{FIR} of the galaxy, assuming the relation of Kennicutt (1998), $\text{SFR}(\text{M}_\odot \text{ yr}^{-1}) = L_{\text{FIR}}/(2.2 \times 10^{43} \text{ erg s}^{-1})$. L_{FIR} (8–1000 μm) is here estimated on the basis of IRAS 12, 25, 60, and 100 μm fluxes using the expression of Sanders & Mirabel (1996); at 12 and 25 μm only upper limits are available, giving L_{FIR} in the interval $1.2\text{--}2.6 \times 10^8 \text{ L}_\odot$, and hence $\text{SFR} \approx 0.02\text{--}0.04 \text{ M}_\odot \text{ yr}^{-1}$, in agreement with the H α estimate.

The age of the current star formation activity can be constrained in a number of ways. Based on the colours of the stellar population, Gallagher et al. (1981) argue that this age should be less than $\sim 4 \times 10^8$ yr, unless the pre-burst system was an intrinsically red inactive dwarf. A lower limit to the age can be estimated if the H α filaments are interpreted as supershells that have cooled and fragmented. Hunter (1996) finds that the age of the bubbles should be at least 6 Myr and, more probably, tens of Myr, based on results from the hydrodynamical simulations of Mac Low, McCray & Norman (1989). A third estimate can be obtained (cf. Heckman 2003; Summers et al. 2004) by assuming that the average mass injection rate into the X-ray bubbles during the starburst roughly corresponds to, or slightly exceeds, the *current* global star formation rate of $\approx 0.03 \text{ M}_\odot \text{ yr}^{-1}$. The derived X-ray gas mass of $\approx 4 \times 10^6 \text{ M}_\odot$ then suggests a bubble age of ~ 100 Myr. Lower filling factors η would imply a lower bubble age according to this argument, but the filling factor for the NGC 1800 wind cannot be reliably estimated from the present data. Simulations (Strickland & Stevens 2000) and *Chandra* observations of the NGC 253 starburst (Strickland et al. 2000) suggest that the wind emission in these cases originates in low filling factor gas, for which $\eta < 50$ per cent, and possibly η could be as low as a few per cent. In the following we will consequently assume a bubble age of ~ 50 Myr.

4.2 X-ray and H α morphology

Although not a robust result due to the low number of detected counts, Fig. 2 suggests the wind is an elongated bipolar outflow, possibly with a conical geometry. Any detailed discussion on the wind morphology is unfortunately not warranted by the data. It is, however, clear from Fig. 2 that the X-ray gas does extend beyond D_{25} , as do the observed H α filaments. Where the northern X-ray emission is lost in the background, a H α web is seen (Hunter 1996), running parallel to the D_{25} major axis for ~ 2 kpc. To the S, a H α loop is detected, interpreted by Hunter (1996) as a supershell extending away from the major axis, based on its size of ~ 500 pc and its shape, with the loop ends extending back towards the main body of the galaxy. In addition, the central regions feature a total of 9–10 ‘fingers’ of H α emission seen on either side of the galaxy, roughly aligned with the minor axis and extending away from the major axis for several hundred pc. Apart from these features Hunter (1996) also detects a larger halo of diffuse ionized gas.

Hunter (1996) suggested that both the northern H α web and the southern loop could be supershells that have expanded out of the plane, cooled, and fragmented. The southern supershell may not yet have cooled and fragmented completely, and could be younger than the N web but would eventually produce a similar structure. The emission-line ratios of the web were found to be consistent with direct photoionization by massive stars being the dominant ionization mechanism. The central H α fingers could be galactic chimneys, providing the low optical depths required for UV photons from massive stars in the disc to traverse the 1–2 kpc to the web. These chimneys could also be funneling hot, X-ray gas above the galactic plane. We note that Norman & Ikeuchi (1989) find for a chimney model of the Milky Way that the chimney phase is associated with a mass flow rate of $0.3\text{--}3 \text{ M}_\odot \text{ yr}^{-1}$. For NGC 1800, these values are likely to be smaller and so probably consistent with the current star formation rate. As noted by Hunter (1996), the time-scales involved would then imply that the H α filaments and fingers have been produced by a previous generation of massive stars rather than the current generation responsible for the observed X-ray emission.

While the emission-line ratios of the H α web generally differ from those expected for collisionally excited gas, it would seem natural to assess to which extent the H α gas may, in fact, be former hot X-gas from the outflowing bubbles that has now cooled to temperatures $\lesssim 10^5$ K. With the estimated cooling time of X-ray gas ($t_{\text{cool}} \sim 1500$ Myr), the upper limit to the age of the current star formation activity of ~ 400 Myr suggests this is not a viable possibility. The even larger discrepancy between t_{cool} and our estimate for the outflow age of a few tens of Myr further strengthens this conclusion. In fact, to produce the mass of the H α

web ($\sim 4 \times 10^7 M_\odot$) with the current mass deposition rate derived for the X-ray gas would require more than a Hubble time. It thus seems unlikely that both the X-ray and H α emission is due to radiative cooling of the wind fluid. This conclusion is similar to that inferred for the NGC 253 starburst (Strickland et al. 2002), and agrees with the result of Hunter (1996) that the H α web is predominantly photoionized. The flux requirements for *pure* photoionization of the web are nevertheless hard to reconcile with the observed H α fluxes. A combination of shock- and photoionization could therefore pose a viable explanation for the H α emission of the web, for example in a scenario where the web is a pre-existing neutral halo cloud that has been moderately shocked by the wind – perhaps somewhat similar to, but brighter than, the X-ray/H α ridge seen well above the disc of M82 (Lehnert, Heckman & Weaver 1999).

4.3 Fate of the diffuse gas

Hunter (1996) conjectures that if the H α features represent fragmenting supershells, it is likely they will break out of the galaxy since they have already reached a large distance (1–2 kpc) from the midplane. For the X-ray gas, the derived cooling time is sufficiently large that radiative losses can be neglected as a first approximation. In that case, gas with an adiabatic index of $\gamma = 5/3$ hotter than

$$T_{esc} = 1.1 \times 10^5 (v_{esc}/100 \text{ km s}^{-1})^2 \text{ K} \quad (2)$$

should be able to escape the galactic gravitational potential (Wang 1995). Modelling the galactic potential as a singular isothermal sphere, the local escape velocity v_{esc} at a distance r from the centre is given by

$$v_{esc}(r) = \sqrt{2}v_{max}[1 + \ln(r_t/r)]^{1/2}, \quad (3)$$

where v_{max} is the maximum rotation velocity, and the potential is truncated at $r = r_t$. With H α having been detected out to 3 times the adopted major radius of D_{25} (Hunter et al. 1994), i.e. ~ 7 kpc, we can conservatively choose $r_t = 50$ kpc. H α observations further suggest $v_{max} \approx 30 \text{ km s}^{-1}$ (LEDA database), yielding $v_{esc} \sim 100 \text{ km s}^{-1}$, and hence $T_{esc} \sim 0.01 \text{ keV}$, for the X-ray gas at either tip of the X-ray emission ellipse D_{spec} ($r \approx 2$ kpc). This is well below the derived gas temperature of $T \simeq 0.25 \text{ keV}$ and suggests that a blow-out of gas from the galaxy is a possibility.

In practice, however, the extended H α halo may prevent blow-out from occurring. Following Summers et al. (2003, 2004), we can evaluate this possibility using the blow-out criterion of Mac Low & McCray (1988). Again neglecting radiative losses, this criterion predicts wind blow-out in a disc galaxy provided that the dimensionless quantity

$$\zeta = 9.4 L_{mech,40} H_{z,kpc}^{-2} P_4^{-3/2} n_0^{1/2} \quad (4)$$

exceeds unity. Here $L_{mech,40}$ is the mechanical energy luminosity of stellar winds and supernova ejecta in units of $10^{40} \text{ erg s}^{-1}$, $H_{z,kpc}$ is the galactic vertical scaleheight in kpc, P_4 is the pressure of the surrounding ISM in units of $P/k = 10^4 \text{ K cm}^{-3}$, and n_0 is the ISM number density in cm^{-3} at the disc midplane. In the case of complete thermalization of the mechanical energy output from supernovae, L_{mech} corresponds to the rate at which the wind thermal energy content E_{th} (Table 4) has been injected over the lifetime of the starburst. Having down-scaled the outflow

age to ~ 50 Myr instead of using the $\eta = 1$ expectation of ~ 100 Myr, we should reduce E_{th} accordingly. This would suggest $L_{mech,40} \approx 0.2$, independently of η . The observed scaleheight can be deduced from the H α profile derived by Hunter et al. (1994), suggesting $H_z \approx 2.5$ kpc. For an exponential atmosphere, the column density $N_{\text{HI}} \sim H_z n_0$, implying $n_0 \approx 0.1 \text{ cm}^{-3}$ for $N_{\text{HI}} \sim 10^{21} \text{ cm}^{-2}$ as suggested by the H α map of Hunter et al. (1994). Conservatively assuming a characteristic ISM temperature of 10^4 K , i.e. $P_4 \approx 0.1$, we then have $\zeta \approx 3$, and the blow-out condition is easily satisfied. While only an indicative result, this clearly suggests as a first approximation that the halo is unable to retain the wind. Moreover, a criterion similar to equation (4), but slightly less strict, is adopted by Koo & McKee (1992) (the constant in equation [4] effectively being ≈ 15 rather than 9.4), which also suggests that for a realistic choice of parameters, the wind may indeed escape NGC 1800 and its H α halo. Any patchiness of the H α halo may further facilitate blow-out along certain directions through the halo.

The question remains whether the ICM, rather than the galactic halo, can confine the wind. Limited work has been done in addressing the impact of external pressure on the possibility of blow-out. One example is the model of Silich & Tenorio-Tagle (2001) in which ICM pressure is taken into account through the way it modifies the ISM distribution, assuming pressure balance at the galaxy–ICM boundary. At the relatively low ICM pressures considered in that study ($P_{ICM}/k = 1$ and 100 K cm^{-3}), it is the mass of any extended gaseous halo, rather than P_{ICM} , which sets the effective minimum value of L_{mech} required for blow-out. For their specific models, a disc-like galaxy with $M_{ISM} \sim 10^8 M_\odot$ and $M_{halo} = 10^8 M_\odot$ (presumably reasonably representative of NGC 1800), embedded in an ICM with $P_{ICM}/k = 100 \text{ K cm}^{-3}$, blow-out demands $L_{mech,40} \gtrsim 0.1$. This result is well in line with our estimate based on equation (4), suggesting that the wind should be able to expand freely into the ambient ICM. It is not clear, however, how to extend the model results of Silich & Tenorio-Tagle (2001) to the exact situation in NGC 1800, given the more subtle dependence on the – in this case unknown – dark matter mass of the galaxy. Moreover, it is also unclear how to extrapolate the results to larger P_{ICM} and how to deal with effects of additional ram-pressure due to the motion of the galaxy through the ICM. Such effects are included in the hydrodynamical simulations of Murakami & Babul (1999). Initially neglecting ram-pressure, these authors find, for a fiducial model dwarf of dark matter mass $M = 10^9 M_\odot$, that a starburst wind confined by ICM thermal pressure reaches a maximum radius of expansion R_{max} which, for $R_{max} \lesssim 2$ kpc (cf. Fig. 2), would correspond to $P_{ICM}/k \gtrsim 5 \times 10^4 \text{ K cm}^{-3}$. For the ICM pressure, our revised group luminosity estimate of $L_X < 10^{41} \text{ erg s}^{-1}$ would imply $T \lesssim 0.4 \text{ keV}$, assuming the L_X – T relation of Helsdon & Ponman (2000). For a $Z = 0.2 Z_\odot$, $T = 0.4 \text{ keV}$ MEKAL plasma, our constraint on L_X translates, via equation (1), into a maximum central ICM density of $N_0 \lesssim 8 \times 10^{-4} \text{ cm}^{-3}$, assuming a group radius of 300 kpc and, conservatively, β -model parameters of $r_c = 50$ kpc and $\beta = 0.5$ (cf. Section 3.3). The resulting ICM thermal pressure, $P/k < 4 \times 10^3 \text{ K cm}^{-3}$, is at least an order of magnitude below that required for confinement of the wind at its current height above the plane. As for ram-pressure, the radial velocity v of NGC 1800 with respect to

the group centre is ~ 400 km s $^{-1}$ (Maia et al. 1989), suggesting $P_{ram} = \rho v^2 \lesssim 1.3 \times 10^{-12}$ dyn cm $^{-2}$ ($\sim 2.5 P_{ICM}$) and hence a total pressure of $P_{tot}/k \lesssim 1.4 \times 10^4$ K cm $^{-3}$. This does not change the conclusion that the outflow probably remains unimpeded by the ICM at present; indeed, the simulations of Murakami & Babul (1999) show that for $P_{ICM}/k = 10^3$ K cm $^{-3}$ and $v = 600$ km s $^{-1}$, a wind is only marginally affected during its expansion phase relative to the case of $P_{ram} = 0$.

As a final test, we can obtain a rough idea about the extent to which the wind is actually confined, by considering the surface brightness structure $S(r)$ of the outflow. A freely expanding, spherically symmetric wind is expected to show a power-law decline in volume density of the wind fluid, $n \propto r^{-\alpha}$, with $\alpha = 2$ and where r is the distance along the outflow (Chevalier & Clegg 1985). A similar behaviour is expected for a conical outflow of constant opening angle, which is perhaps more relevant for NGC 1800. A power-law fit, $S \propto r^{-\gamma}$, to the 0.3–2 keV profile shown in Fig. 3 gives $\gamma \approx 1.3 \pm 0.1$ for both the northern and southern ends of a conical outflow. Since, at fixed cone height r , the line of sight through the cone grows with r , we have $S(r) \propto n^2 r$ for an isothermal wind expanding in a regular cone, and hence $\alpha = (\gamma + 1)/2 \approx 1.15$. Temperature variations within the wind would have limited impact on this result, since S is roughly independent of T at the relevant temperatures (~ 0.25 keV) and energies (0.3–2 keV). The freely expanding winds of M82 and NGC 253 show values of $\alpha = 0.9$ and 1.3, respectively, thus bracketing our estimate of $\alpha \approx 1.15$. By contrast, NGC 3077, in which X-ray and H α images suggest that the hot X-ray bubbles are indeed confined by H α gas, shows a value $\alpha \approx 0.6$ (see Ott et al. 2003 for a discussion of the results for these three galaxies). Overall, this seems to indicate that the wind of NGC 1800 is not substantially confined.

Summarizing, there is no indication of significant confinement from the surface brightness structure of the wind, a result clearly supported both by models and simulations of dwarf galaxy winds expanding into an ambient medium of the relevant pressures. The above considerations suggest that the wind, currently appearing to be breaking out of the galactic plane, will eventually blow out through the galactic halo, probably delivering energy and newly synthesized metals to the ICM. This would be particularly true if the very hot wind fluid, presumably remaining undetected in these observations but carrying most of the wind energy and metals (cf. Strickland & Stevens 2000), can have terminal outflow velocities much larger than those of the X-ray detectable gas (e.g. Heckman 2003).

5 SCALING PROPERTIES OF DWARF STARBURST GALAXIES

Due to their X-ray faintness, detailed X-ray studies of dwarf galaxies have generally not been feasible prior to the advent of *Chandra* and *XMM-Newton*. Consequently, the small number of dwarf starbursts studied in X-rays so far has precluded any statistical investigation of their X-ray properties, although Hartwell et al. (2004) discussed some properties of the three dwarf starbursts NGC 4214, NGC 4449, and NGC 5253. To amend this situation, the derived prop-

erties of NGC 1800 are here compared to those of other dwarf starbursts and to starburst galaxies in general, and a first detailed discussion is presented of the X-ray properties of all dwarf starburst galaxies that have so far been subjected to detailed X-ray studies and in which, to our knowledge, diffuse X-ray emission has been unambiguously detected.

In Table 5 we list some properties of these dwarf starbursts and the associated references to published X-ray data. We have assumed distances D as given in the reference in the Table, and B -band luminosities from Tully (1988), corrected to these distances, with uncertainties based on those of the apparent magnitudes as listed by de Vaucouleurs, de Vaucouleurs & Corwin (1976) (for NGC 625, no values are provided). Note that NGC 1800 is the most distant dwarf starburst having diffuse X-ray emission safely detected so far (Thuan et al. 2004 report marginal *Chandra* detections of diffuse emission in the $D = 54.3$ Mpc and $D = 12.6$ Mpc dwarfs SBS 0335-052 and I Zw 18, but at a level of just 8 ± 5 and 23 ± 7 diffuse source counts, respectively). K_s band luminosities in the Table have been computed for D from the total K_s magnitude of the galaxy as listed in the 2MASS Extended Sources Catalog³. The far-infrared (40–120 μ m) luminosities L_{FIR} have been calculated from the 60 μ m and 100 μ m fluxes S_{60} and S_{100} and their errors as listed in the IRAS Galaxy Catalog (Fullmer & Lonsdale 1989), using the relation of Devereux & Eales (1989):

$$L_{FIR} = 3.65 \times 10^5 [2.58S_{60}(\text{Jy}) + S_{100}(\text{Jy})] D^2 (\text{Mpc}) L_\odot. \quad (5)$$

An exception is NGC 4449 which is not listed in the IRAS Galaxy Catalog. Instead we adopt the 10–150 μ m value also used by Summers et al. (2003). We have chosen not to attempt to correct this value to the 40–120 μ m band, as the typical FIR spectral energy distribution of local starbursts rises sharply between ~ 10 –100 μ m and then declines, making the difference between the two bands relatively small (e.g. Spinoglio et al. 2002).

The reason for tabulating L_{FIR} , L_B , and L_K along with the X-ray luminosity of the diffuse gas, is that L_{FIR} is known to be a tracer of the star formation rate (Section 4.1) and as such might be related to the diffuse X-ray luminosity from the ISM and a starburst wind. Also, L_K should provide a reliable measure of stellar mass, but for comparison with Read & Ponman (2001) we also examine dependencies on L_B , although this quantity is more affected by the presence of young stellar populations and dust. Following Read & Ponman (2001), we can then define the 'activity' of the galaxy as the star formation rate per unit stellar mass, measured by L_{FIR}/L_B , or even better, L_{FIR}/L_K .

Inspired by the multivariate statistical study of Read & Ponman (2001, hereafter RP01) on normal (i.e. low-activity) dwarfs and non-dwarf starbursts, we have performed the first investigation of the X-ray scaling properties of dwarf starbursts with well-studied diffuse X-ray emission. To bring all galaxies on an equal footing and obtain consistency with RP01, we have converted dwarf X-ray luminosities to the 0.1–2 keV band, assuming a MEKAL plasma with $Z = 0.2Z_\odot$ at the relevant temperature. Linear regression fits for the parameter combinations under study (in

³ <http://irsa.ipac.caltech.edu/applications/2MASS/PubGalPS/>

Table 5. Summary of properties of dwarf starbursts. X-ray luminosities are total values for the diffuse gas only.

| Galaxy | D (Mpc) | L_X (10^{38} erg s $^{-1}$) | L_{FIR} (10^8 L $_{\odot}$) | L_B (10^8 L $_{\odot}$) | L_K (10^8 L $_{\odot}$) | References |
|----------|--------------|--------------------------------------|--------------------------------------|----------------------------------|----------------------------------|------------------------|
| NGC 625 | 3.9 | $\sim 1.0^a$ | 1.3 ± 0.1^i | 5.4 | 9.0 ± 0.4 | Bomans & Grant (1998) |
| NGC 1569 | 2.2 | 8.2^b | 3.5 ± 0.4^i | 10.4 ± 0.6 | 7.5 ± 0.2 | Martin et al. (2002) |
| NGC 3077 | 3.6 | $20-50^c$ | 1.4 ± 0.1^j | 12.8 ± 1.0 | 33.6 ± 0.6 | Ott et al. (2003) |
| NGC 4214 | 2.9 | 3.5 ± 0.3^d | 2.4 ± 0.3^i | 11.7 ± 0.9 | 12.7 ± 0.6 | Hartwell et al. (2004) |
| NGC 4449 | 2.9 | 9.1 ± 0.6^d | 9.5^k | 17.4 ± 1.0 | 23.2 ± 0.8 | Summers et al. (2003) |
| NGC 5253 | 3.2 | 3.9 ± 0.3^e | 3.9 ± 0.4^i | 7.0 ± 0.6 | 10.3 ± 0.3 | Summers et al. (2004) |
| NGC 1800 | 7.4 | 1.3 ± 0.3^f | 0.8 ± 0.1^i | 5.0 ± 0.4 | 9.7 ± 0.5 | This study |

Notes: ^a0.1–2.4 keV. Uncertainties on L_X are not available for this galaxy. ^b0.3–6 keV; uncertainties on L_X are not available. ^c L_X varies from $20-50 \times 10^{38}$ erg s $^{-1}$ depending on the spectral model assumed. ^d0.3–8 keV. ^e0.37–6.0 keV. This galaxy also displays spectral evidence for a diffuse power-law component, possibly due to unresolved point sources; the quoted value is for the thermal components alone. ^f0.3–3 keV. ⁱ40–120 μ m, see text for details. ^j40–120 μ m; Yun (1999) lists a value 2.7×10^8 L $_{\odot}$ in an unspecified band. ^k10–150 μ m (Summers et al. 2003), see text.

logarithmic space) have been conducted using different regression methods (Isobe et al. 1990). Results for orthogonal regression fits are presented in Table 6; only those parameter combinations yielding acceptable fits are reproduced in the Table, taken to be those fits for which the results of different regression techniques – orthogonal regression, ordinary least-squares (OLS), OLS bisector, mean OLS, and reduced major-axis – gave consistent results. Also listed in the Table is the value of the Spearman rank-order correlation coefficient r_s (in the range $[-1; 1]$) and the significance t_s of r_s being non-zero (see e.g. Press et al. 1996).

5.1 X-ray vs optical and far-infrared luminosities

We plot in Fig. 6a a comparison of the far-infrared and diffuse X-ray luminosities of these dwarf starbursts. Also plotted for comparison are the eight non-dwarf starbursts in the sample of RP01, defined by these authors as those galaxies having $L_{FIR} > 0.38L_B$ (with L_{FIR} also derived via equation [5]). To be able to compare our results directly to those of RP01, we use L_B as the third parameter of investigation but compare the results to those obtained using L_K below. There is, in fact, a tight correlation between L_B and L_K for *all* the galaxies shown in the figure ($r_s = 0.93$, $t_s = 9.0$), suggesting that L_B may indeed be used as a proxy for the stellar mass of these galaxies. With one notable exception (NGC 3077), L_X is seen to correlate with L_{FIR} for the dwarfs, as was found by RP01 for non-dwarfs and quiescent galaxies. The dwarf correlation seems to match well that derived for such galaxies, leading to a remarkably tight correlation ($t_s = 11.3$) across three orders of magnitude in L_{FIR} for the combined sample of dwarf and normal starburst galaxies. NGC 1800 lies at the low end of the range in L_X and L_{FIR} spanned by the dwarf starbursts, but is otherwise fairly typical, fitting perfectly well to the correlation derived for the full starburst sample. Taken as a whole, L_X and L_{FIR} for the dwarf starbursts are well matched to values for normal non-dwarf spirals but lie substantially below those of non-dwarf starbursts. These results are to be expected, if the observed diffuse X-ray emission is indeed associated with the global level of star formation. In Fig. 6b we plot correspondingly L_X and L_B . There is a clear correlation

between these two parameters for the dwarf starbursts ($t_s = 4.4$). This correlation appears to be somewhat steeper than is the case for non-dwarf starbursts, but not highly significantly so if NGC 3077 is excluded from the dwarf sample (the regression slopes then being consistent at the $\sim 2\sigma$ level). The reasonable match between the dwarf and non-dwarf correlations again lead to a tight correlation for the combined sample ($t_s = 9.8$, with M82 excluded) across two orders of magnitude in L_B . The correlations are less significant when using L_K instead of L_B , with $t_s = 1.9$ for dwarfs, 2.2 for non-dwarfs, and 8.1 for the combined sample. The dwarf regression slope $m = 2.85 \pm 0.96$ is also in this case steeper than that of normal starbursts, ($m = 0.98 \pm 0.40$), but again consistent with it at the $\sim 2\sigma$ level.

In Fig. 7a the quantity measuring galaxy activity (L_{FIR}/L_K) is plotted against stellar mass (L_K). No clear correlation is seen, with $t_s = -0.9$ for dwarfs and -0.4 for the entire sample, giving unacceptable regression fits. This is analogous to the result for the larger and more general sample of RP01 based on *B*-band luminosities. It implies that we may separate the impact of mass and activity on our results. As can be seen, the activity of NGC 1800 lies at the low end of typical starbursts (cf. also Fig. 6a). The 'mass-normalized' X-ray luminosity L_X/L_K as plotted in Fig. 7b does not show a clear correlation with L_K either ($t_s = 0.2$ for dwarfs, -0.7 for normal starbursts, and -1.5 for the full sample, producing unacceptable fits in all cases). This is again consistent with the results of RP01 for more massive starbursts, using L_B rather than L_K , whereas the 'normal', i.e. quiescent, galaxies of that study display a strong correlation ($t_s = 4.7$). The position of NGC 1800 in Fig. 7b is not conspicuous and demonstrates no evidence for enhanced wind luminosity due to compression of the wind fluid by ICM confinement. NGC 1569 and NGC 3077, on the other hand, appear to have a somewhat higher L_X/L_K ratio than the remaining starbursts.

When plotted against the star formation 'activity' L_{FIR}/L_K in Fig. 8, L_X/L_K of the dwarf starbursts does seem to show a dependence, albeit a weak one, and again with NGC 3077 clearly deviating from the common trend (this galaxy must be excluded in order to obtain an acceptable fit for the dwarfs alone). Aside from NGC 3077,

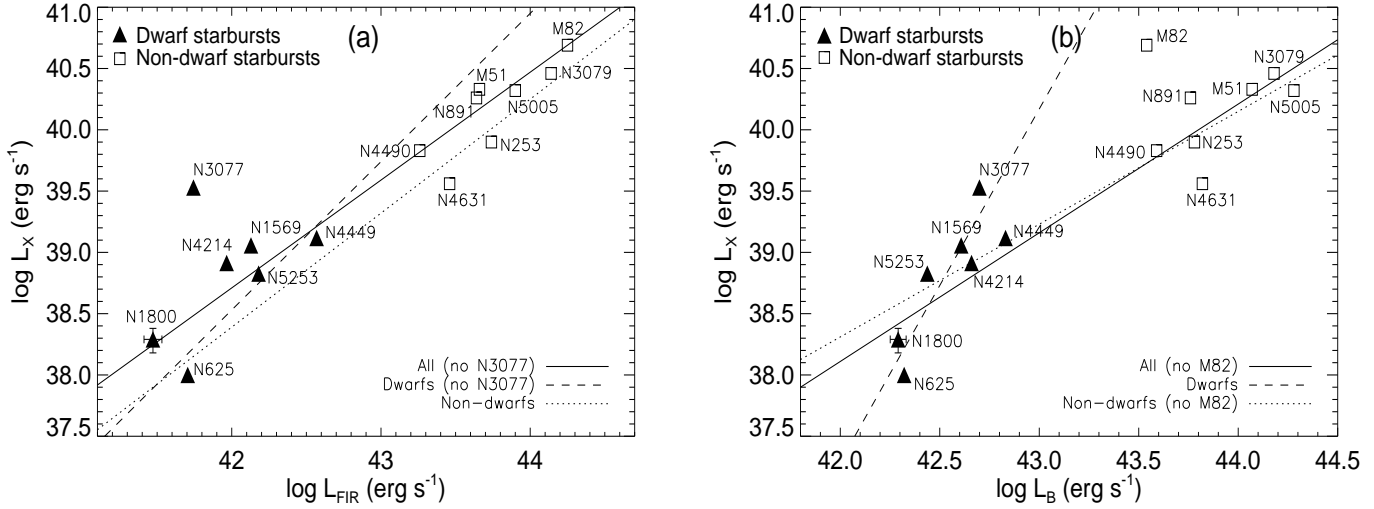


Figure 6. Diffuse L_X along with far-infrared luminosity L_{FIR} (a), and B -band luminosity L_B (b) for starburst galaxies. Dotted lines are the best-fitting relations of Read & Ponman (2001) to *ROSAT* 0.1–2 keV data of a subsample of eight starburst spirals, $\log L_X = (0.93 \pm 0.26) \log L_{FIR} - (0.67 \pm 0.22)$, and (excluding M82) $\log L_X = (0.92 \pm 0.42) \log L_B - (0.33 \pm 0.26)$. Dashed lines represent the relations obtained from our regression analyses of the dwarf subsample (see Table 6), and solid lines those derived for the full (dwarf + non-dwarf) sample. For clarity in these and the following figures, typical error bars for the dwarf galaxies (cf. Table 5) are shown for NGC 1800 only.

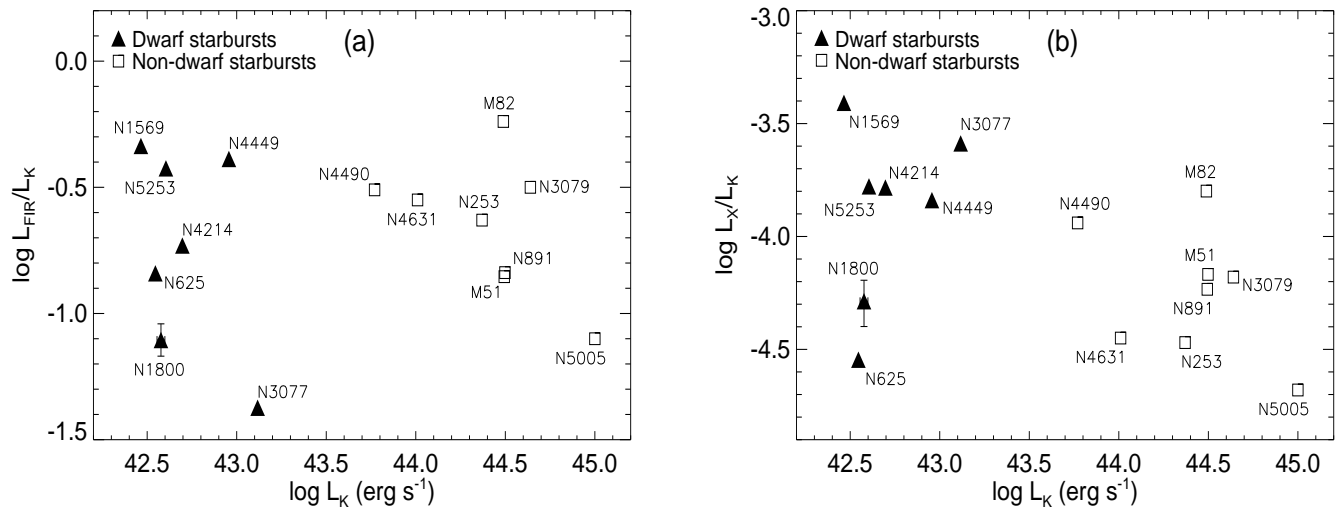


Figure 7. Star formation 'activity' L_{FIR}/L_K (a) and 'mass-normalized' X-ray luminosity L_X/L_K (b) as a function of galactic stellar 'mass' L_K .

the dwarf starbursts conform to the relation found for the starburst sample of RP01. Again, NGC 1800 seems to be fairly typical of the dwarf starburst population, which, in terms of absolute numbers, is similar to non-dwarf starbursts in this representation but shows slightly higher values on both axes than do quiescent spirals. If using L_B rather than L_K as a tracer of stellar mass, the correlations between activity and mass-normalized L_X become less significant ($t_s = 1.7$ for dwarfs and 2.1 for the combined sample), with comparable regression slopes for dwarfs and

normal starbursts, as seen from Table 6 and from the relation derived by RP01 for their sample, $\log L_X/L_B = (0.96 \pm 0.23) \log L_{FIR}/L_B - (3.59 \pm 0.23)$. Interestingly, it also appears that dwarf starbursts generally have lower values of L_{FIR}/L_B (in the range $[-1.0; -0.25]$) compared to normal starbursts ($[-0.4; 0.7]$). As can be seen from Fig. 8, there is no such indication for L_{FIR}/L_K , suggesting that the effects of relatively stronger dust obscuration in larger galaxies is responsible. In addition, dwarf starbursts are low-metallicity objects due, at least in part, to their shallow

gravitational potentials. Assuming a dust-to-gas mass ratio which is proportional to metallicity (Lisenfeld & Ferrara 1998; Galliano et al. 2003), dwarf starbursts would thus on average suffer considerably less obscuration than larger starbursts, as observed.

NGC 3077 seems to deviate somewhat from the common trend depicted in Figs. 6a and 8. This galaxy is a member of a group/triplet consisting also of M81 and the prototypical starburst M82. There is substantial HI evidence that these three galaxies are tidally interacting, and these interactions are believed to have triggered the starburst activity in both NGC 3077 and M82 (see e.g. Ott et al. 2003). It is suggested by Figs. 6–8 that NGC 3077 exhibits a current star formation activity which is at the low end of typical dwarf starbursts, while at the same time displaying a rather high X-ray luminosity. This seems particularly true in light of the fact that we have plotted the *lowest* value of L_X allowed by the analysis of Ott et al. (2003). Oddly, this result is exactly opposite to that derived by Read & Ponman (1998) on high-activity merging and interacting systems, in which a *deficit* of X-ray emission relative to L_{FIR} was found in the most active systems. The physical scale of soft diffuse emission in NGC 3077 is less than 1 kpc, but the *Chandra* observations of Ott et al. (2003) show no evidence of strong nuclear non-stellar activity. Any AGN would remain largely hidden in X-rays, since only ~ 15 per cent of all X-ray emission within this galaxy originates in resolved point sources. A hidden AGN would presumably be dust-enshrouded and so should radiate strongly in the FIR, for which there is no evidence in Figs. 6–8. It is possible that the star formation rate of NGC 3077 has recently declined, and that we are currently seeing hot gas generated from star formation which took place a few Myr ago. This is, in fact, in line with the results of Ott et al. (2003) who find that the hot bubble properties in NGC 3077 suggest a star formation rate of $\sim 0.6 \text{ M}_\odot \text{ yr}^{-1}$, an order of magnitude above the current SFR of $0.06 \text{ M}_\odot \text{ yr}^{-1}$ as derived from H α and FIR fluxes (note also that a rise in L_{FIR} by a factor of ~ 10 would actually drop NGC 3077 on to the general trends shown in Figs. 6a and 8). With an estimated bubble age in NGC 3077 of 2–10 Myr, this may indicate that the SFR of this galaxy has declined considerably within the last few Myr, and that the observed X-ray luminosity to a large degree reflects previous rather than current star formation activity.

5.2 Dependencies on gas temperature

Motivated by the presence of scaling relations between T of X-ray gas and e.g. L_X and mass derived for galaxy groups and clusters, we plot in Fig. 9 the diffuse X-ray luminosities, hot gas masses, and galactic stellar ‘masses’ as functions of the hot gas temperature T . The situation is complicated slightly by the presence of a second thermal component in some systems. Here the two components are plotted separately where possible. Fig. 9a shows L_X versus T , in which, again, NGC 1800 resumes a fairly typical position. When excluding NGC 3077 from the dwarf sample, there is marginal evidence ($t_s = 1.2$) for L_X correlating with T for these galaxies. There is a much stronger trend for the normal starburst subsample ($t_s = 5.7$ with NGC 891 excluded, see below), which is also reflected in the high statistical significance of the full-sample relation ($t_s = 5.4$, again excluding

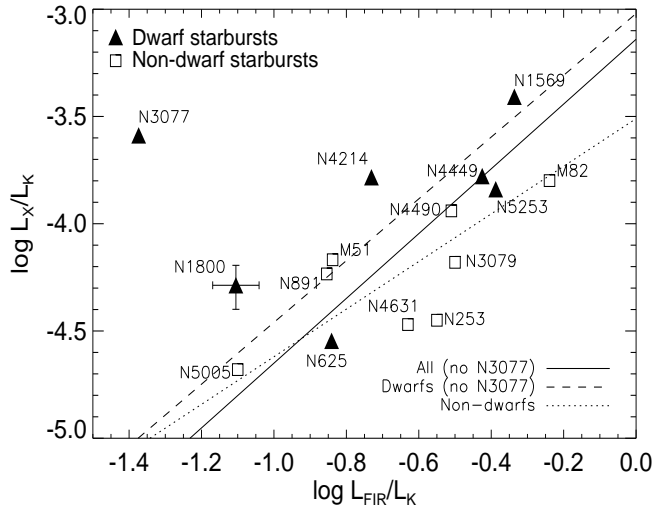


Figure 8. Diffuse L_X and far-infrared luminosity L_{FIR} for starbursts, ‘mass-normalized’ using L_K . Lines have the same meaning as for Fig. 6a.

NGC 891). For the hotter of the two thermal components there is again a suggestive trend ($t_s = 1.2$), but any comparison to the behaviour of the cold component in dwarfs or to normal starbursts is hampered by the small numbers involved. While this restriction also inhibits any firm conclusions for the cold component, the position of the best-fitting relation for the RP01 starbursts does seem to indicate that dwarf bursts are slightly hotter than would be suggested by an extrapolation of this relation to lower X-ray luminosities. However, also evident from Fig. 9a is that in systems where a second, hotter thermal component has been detected, the colder component dominates the soft X-ray output (and hot gas mass, as discussed below). This probably explains why systems in which only one component is detected tend to have T consistent with that of the colder component in two-component systems. It could be speculated that more sensitive observations would reveal evidence for a hot secondary component in most, if not all, systems, including the normal starbursts in Fig. 9a observed by *ROSAT*. If so, the indication that dwarfs are hotter than expected from normal starbursts could be an artefact of splitting L_X and T of the dwarfs into two components. But, as can be judged from Fig. 9a, even if adding L_X of the hot component to that of the cold component while assuming $T \equiv T_{cold}$, all dwarfs (exempting NGC 3077) still lie at or to the right of the normal starburst regression line shown in the figure.

In Fig. 9b, T is correspondingly plotted along with the mass $M_{gas}\eta^{1/2}$ of X-ray emitting gas. Again, where a second thermal component has been detected, values published for both components are plotted. NGC 625 is not included, because it lacks a published value for M_{gas} . Aside from the wind geometry assumed in the published analyses (an ellipsoidal volume for NGC 1800, cylindrical ones for NGC 1569 and NGC 4214, and a spherical geometry for the remainder), the plotted gas masses M_{gas} have all been consistently derived as outlined in Section 4.1. Hence, Fig. 9b should provide a fair comparison between different galaxies assum-

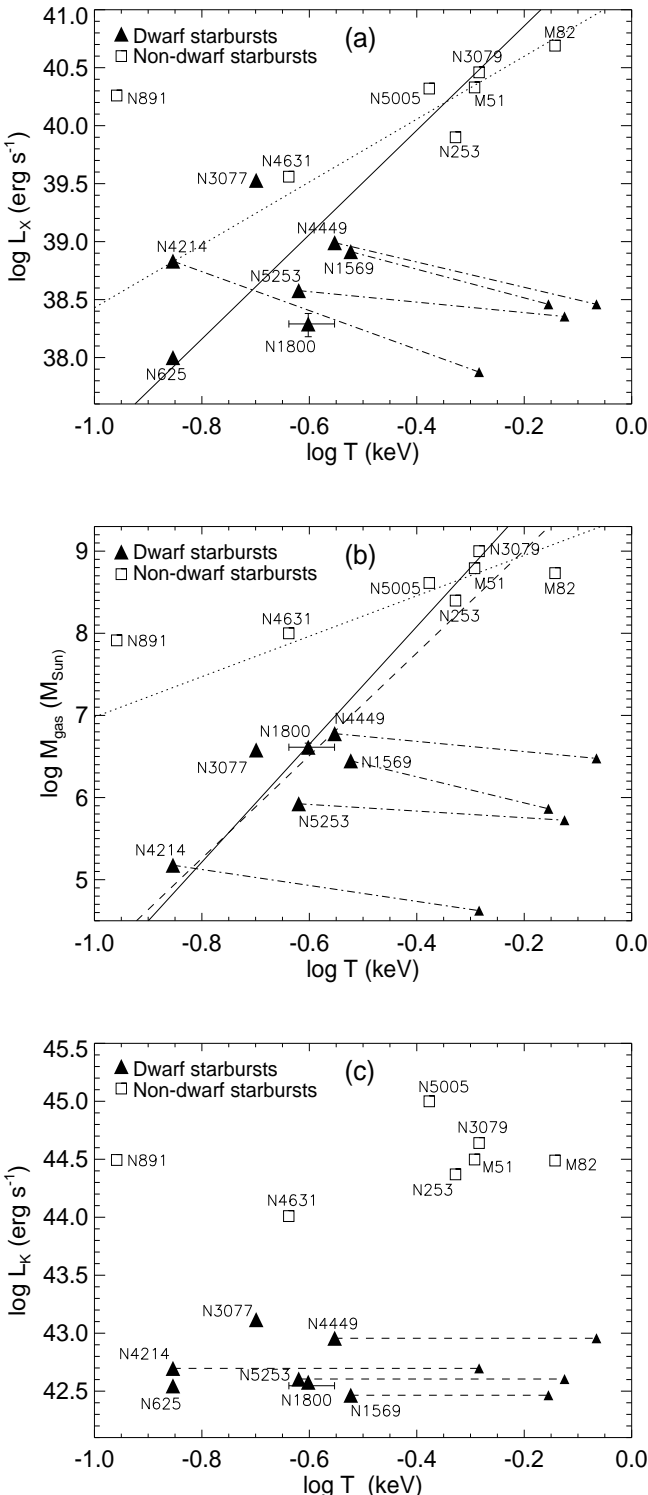


Figure 9. Temperature of the diffuse gas along with its X-ray luminosity L_X (a), mass $M_{\text{gas}}\eta^{1/2}$ (b), and the galactic 'mass' L_K (c). Where values for a second thermal component have been published, this component is shown with smaller symbols, connected to the colder component by dash-dotted lines. Lines have the same meaning as for Fig. 6a, except that NGC 891 has been omitted from the regression analyses of the non-dwarf and full samples in Fig. 9a and 9b, whereas NGC 3077 is included in the dwarf and full samples of Fig. 9b. Errors on M_{gas} for NGC 1800 are based on the fractional errors on the spectral normalization.

ing that the filling factor η does not vary substantially between them. Note, however, that the value for NGC 3077 as derived by Ott et al. (2003) assumes $Z = Z_\odot$. With resulting M_{gas} scaling as $Z^{-0.5}$, the plotted value for this galaxy is thus a lower limit for any subsolar metallicity (but note also that the ionized ISM of NGC 3077 has Z close to solar; Calzetti et al. 2004). Though dealing with small numbers, there seems to be a weak tendency for dwarfs with larger gas mass to display hotter gas, and this applies to both the 'cold' ($t_s = 1.3$) and 'hot' ($t_s = 1.9$) thermal components (RP01 find a more significant trend, $t_s = 3.9$, for their starbursts). The correlation does not seem to arise from a scaling with total galaxy mass for either component, as can be judged from Fig. 9c (for the cold component, $t_s = -0.5$ for dwarfs and 0.4 for normal starbursts, and $t_s = 0.6$ for the hot component in dwarfs), although the combined sample shows a marginally significant trend ($t_s = 1.8$, which however reduces to $t_s = 1.0$ if NGC 891 is removed from the sample). Again, dwarf winds appear to be hotter for a given gas mass than expected on the basis of starbursts in more massive galaxies, an indication which, once more, cannot be explained simply by our splitting of the X-ray gas in some dwarfs into two components.

Mainly due to its low gas temperature, NGC 891 is seen to fall well outside the (L_X, T) and (M_{gas}, T) regions occupied by other starburst galaxies. Although the galaxy is actively forming stars at present and further shows evidence for extraplanar diffuse X-ray emission which is possibly related to star formation processes in the disc, it remains unclear whether this emission represents an outflowing galactic wind (see the discussion in Strickland et al. 2004, who furthermore derive a mean temperature of $T = 0.23$ keV for the off-disc gas, as opposed to $T = 0.11 \pm 0.03$ keV found by RP01 for the diffuse emission). Moreover, the FIR 'temperature' S_{60}/S_{100} of the galaxy is only 0.31, placing it in the 'normal' (quiescent) rather than 'starburst' subsamples of Kennicutt (1998) and Strickland et al. (2004). Finally, the galaxy shows evidence for a hot halo extending to ~ 5 kpc above the disc. The gas temperature listed by RP01 for this galaxy is likely to reflect the properties of this corona-like gas to a significant degree (see also Read et al. 1997). Given these circumstances, it seems sensible to exclude NGC 891 from regression analyses involving T of the X-ray gas in starbursts. NGC 4490 is also excluded in this context, as no value of T has been published for this galaxy.

5.3 Dwarf vs normal starbursts

An overall conclusion of the above comparisons, which is identical to that arrived at by RP01 for non-dwarf starbursts, is that the diffuse X-ray emission in dwarf starbursts seems to be related to star formation activity rather than galactic (stellar) mass. This contrasts with the results for quiescent spirals but is in line with properties of more massive starbursts. While there is an indication (at the $\sim 2\sigma$ level) that the diffuse L_X of dwarf starbursts has a steeper dependence on L_B or L_K than in 'normal' starbursts, dwarf starbursts as a class appear to conform to the scaling relations obeyed by normal starburst galaxies. Dwarf bursts can therefore, to a large degree, be considered down-scaled versions of normal starburst galaxies. Whether the properties of NGC 1800 are affected by being in a group or not, is

Table 6. Selected results of regression analyses assuming relations of the form $Y = mX + c$, with X and Y unweighted. Errors on the regression coefficients m and c are 1σ . Column 3 specifies the subsample used (D = dwarfs, N = normal starbursts from Read & Ponman 2001, All = D + N) and the number [N] of galaxies in the subsample. Column 6 gives the Spearman rank-order correlation coefficient r_s , and column 7 its significance t_s (see text for details). Column 8 specifies the figure depicting the derived relation. L_X is assumed to be in the 0.1–2 keV band.

| Y | X | Galaxy sample [N] | m | c | r_s | t_s | Fig. |
|---------------------|--------------------|------------------------------|------------------|-------------------|-------|-------|------|
| $\log L_X$ | $\log L_{FIR}$ | D [7] | 2.01 ± 1.48 | -45.45 ± 0.60 | 0.50 | 1.3 | – |
| $\log L_X$ | $\log L_{FIR}$ | D, no N3077 [6] | 1.21 ± 0.38 | -12.29 ± 0.24 | 0.77 | 2.4 | 6a |
| $\log L_X$ | $\log L_{FIR}$ | All [15] | 0.82 ± 0.09 | 4.41 ± 0.20 | 0.93 | 9.0 | – |
| $\log L_X$ | $\log L_{FIR}$ | All, no N3077 [14] | 0.88 ± 0.07 | 1.75 ± 0.13 | 0.96 | 11.3 | 6a |
| $\log L_X$ | $\log L_B$ | D [7] | 2.88 ± 0.59 | -83.67 ± 0.14 | 0.89 | 4.4 | 6b |
| $\log L_X$ | $\log L_B$ | D, no N3077 [6] | 2.36 ± 0.54 | -61.50 ± 0.14 | 0.89 | 3.8 | – |
| $\log L_X$ | $\log L_B$ | All [15] | 1.15 ± 0.15 | -10.09 ± 0.15 | 0.85 | 5.9 | – |
| $\log L_X$ | $\log L_B$ | All, no M82 [14] | 1.05 ± 0.11 | -5.99 ± 0.15 | 0.94 | 9.8 | 6b |
| $\log L_{FIR}/L_K$ | $\log L_K$ | N [8] | -0.53 ± 0.23 | 22.87 ± 0.15 | -0.40 | -1.1 | – |
| $\log L_X/L_B$ | $\log L_{FIR}/L_B$ | D, no N3077 [6] | 1.49 ± 0.96 | -3.05 ± 0.34 | 0.66 | 1.7 | 8 |
| $\log L_X/L_B$ | $\log L_{FIR}/L_B$ | All [15] | 0.89 ± 0.26 | -3.42 ± 0.23 | 0.29 | 1.1 | 8 |
| $\log L_X/L_B$ | $\log L_{FIR}/L_B$ | All, no N3077 [14] | 0.95 ± 0.17 | -3.48 ± 0.14 | 0.52 | 2.1 | 8 |
| $\log L_X/L_K$ | $\log L_{FIR}/L_K$ | D, no N3077 [6] | 1.44 ± 0.47 | -3.02 ± 0.28 | 0.77 | 2.4 | – |
| $\log L_X/L_K$ | $\log L_{FIR}/L_K$ | N [8] | 1.11 ± 0.16 | -3.51 ± 0.13 | 0.69 | 2.3 | – |
| $\log L_X/L_K$ | $\log L_{FIR}/L_K$ | All, no N3077 [14] | 1.51 ± 0.36 | -3.14 ± 0.20 | 0.71 | 3.4 | – |
| $\log L_{X,cold}$ | $\log T_{cold}$ | N, no N4490/N891 [6] | 2.71 ± 0.48 | 41.14 ± 0.20 | 0.94 | 5.7 | 9a |
| $\log L_{X,cold}$ | $\log T_{cold}$ | All, no N4490/N891 [13] | 4.50 ± 0.60 | 41.76 ± 0.28 | 0.85 | 5.4 | 9a |
| $\log L_{X,hot}$ | $\log T_{hot}$ | D [4] | 3.25 ± 0.50 | 38.80 ± 0.01 | 0.63 | 1.2 | – |
| $\log M_{gas,cold}$ | $\log T_{cold}$ | D, no N625 [6] | 6.25 ± 1.37 | 10.26 ± 0.31 | 0.54 | 1.3 | 9b |
| $\log M_{gas,cold}$ | $\log T_{cold}$ | N, no N4490/N891 [6] | 2.46 ± 0.65 | 9.44 ± 0.18 | 0.77 | 2.4 | 9b |
| $\log M_{gas,cold}$ | $\log T_{cold}$ | All, no N891/N4490/N625 [12] | 7.17 ± 0.92 | 10.95 ± 0.33 | 0.83 | 4.7 | 9b |
| $\log M_{gas,hot}$ | $\log T_{hot}$ | D [4] | 8.55 ± 0.25 | 7.02 ± 0.06 | 0.80 | 1.9 | – |

not easily addressed by these comparisons, given the small size of our dwarf starburst sample. Specifically, it could be imagined that the wind X-ray luminosity of NGC 1800 could be enhanced due to compression by the ambient group ICM, but there is no such hint to be taken from Figs. 6–8.

The only notable difference between dwarf and normal starbursts emerging from these results is that the winds of dwarfs appear to be somewhat hotter than expected from an extrapolation of normal starbursts to lower L_X and, particularly, M_{gas} (Figs. 9a and 9b). One possible explanation is that there is a lower limit to the temperature generated in superbubbles, perhaps at $T \approx 0.10$ –0.15 keV, which is independent of galactic environment. An alternative is that *Chandra* is not sensitive to cooler gas, so that a powerful selection effect is at work on the derived gas temperatures. To investigate this, we performed a PIMMS calculation, assuming a $Z = 0.2Z_\odot$ plasma subjected to an absorbing column density $N_H = 3 \times 10^{20} \text{ cm}^{-2}$. For a fixed, unabsorbed 0.3–2 keV flux arriving at the ACIS-S detectors, $T \approx 0.6$ keV would maximize the observed 0.3–2 keV count rate. Compared to this, 80 per cent of the incoming photons remain undetected for $T = 0.1$ keV (with 50 per cent at $T = 0.2$ keV and 65 per cent at $T = 0.15$ keV). To safely detect low- T components in starburst winds (characteristic tem-

peratures $\lesssim 0.10$ keV) in typical *Chandra* observations, these components would therefore have to be intrinsically brighter than the entire NGC 1800 wind by an order of magnitude. In the present X-ray dwarf sample, only the wind of the unusual NGC 3077 has the potential to meet this requirement. This suggests that superbubble gas at such low temperatures would remain undetected, and therefore that the apparent differences between dwarf and normal starbursts may be a result of observational selection effects. Support for this view comes from the different simulations of Strickland & Stevens (2000), in which very low- T gas is present (down to $T \sim 10^5$ K), but the corresponding *characteristic* emission-weighted temperature as it would be inferred from *ROSAT* PSPC data is always $\gtrsim 0.10$ keV. Any clear detection of very low temperature gas in starburst winds would help resolve the issue.

6 SUMMARY

Diffuse X-ray emission has been unambiguously detected in NGC 1800, the most distant dwarf starburst galaxy for which this has yet been reported. The diffuse emission, with a 0.3–3 keV luminosity of $1.3 \pm 0.3 \times 10^{38} \text{ erg s}^{-1}$, accounts

for at least 60 per cent of the total soft X-ray output of the galaxy, with the remainder being contributed by five resolved point sources. Two of these sources are located at the optical outskirts of the galaxy and may be unassociated with NGC 1800 (possibly being background AGN), whereas the remaining three have X-ray luminosities consistent with X-ray binaries. The morphology of diffuse emission suggests an elongated outflow of hot ($T \simeq 0.25$ keV) gas, similar to the winds seen in more nearby starburst galaxies, and reaching distances of ~ 2 kpc above the galactic plane. The northern tip of the diffuse X-ray emission coincides with an extended H α structure. We suggest a scenario in which photoionization from massive stars in the disc combines with shock ionization due to the expanding wind, in producing and maintaining the H α emission of this structure. There is no evidence for a hot, gaseous halo surrounding the galaxy, implying an upper limit to the X-ray luminosity of such a halo in agreement with expectations from simulations of disc galaxy formation.

NGC 1800 is embedded in a small galaxy group, but we are unable to detect any X-ray emission from intragroup gas, deriving an upper limit to the group X-ray luminosity of $L_X < 10^{41}$ erg s $^{-1}$. There is no clear evidence that the outflowing wind of NGC 1800 is currently interacting with any hot intracluster medium in the group. Mechanical considerations suggest that the wind will probably be able to escape the extended H I halo of the galaxy, particularly if the halo has a patchy distribution. Models including external pressure from intragroup gas suggest that the observable component of the hot wind will not become confined by this gas either, thus enabling the injection of wind energy and newly synthesized metals into the group ICM.

A first comparative study of the diffuse X-ray emission from dwarf starbursts as a class has been carried out. While lying at the low end of the X-ray luminosity range spanned by dwarf starbursts with detected X-ray emission, NGC 1800 seems to be fairly typical of the small population studied in X-rays so far. We find that diffuse X-ray emission in these systems is related to starburst activity rather than galaxy mass, equivalent to results inferred for more massive starburst galaxies. Specifically, there is a clear correlation between the mass-normalized X-ray and far-infrared luminosities, whereas the mass-normalized X-ray luminosity is largely independent of galaxy mass. In this and other respects, the investigated properties of dwarf starbursts seem roughly consistent with an extrapolation to lower masses of starbursts in non-dwarf galaxies. The X-ray luminosity and mass of the hot X-ray emitting gas in dwarfs appear to scale weakly with emission-weighted mean temperature of this gas, a correlation which does not seem to arise from a scaling of gas temperature with total galaxy mass. This indicates that the hot gas is far from being in hydrostatic equilibrium in such systems, consistent with the observed morphology of the gas. In some systems, two thermal components are seen, but always with the colder of the two components dominating the hot gas mass and diffuse X-ray emission. Interestingly, there is a clear indication that the X-ray gas in dwarf starbursts is generally hotter than would be expected from an extrapolation of normal starbursts to low L_X and M_{gas} . However, it cannot be ruled out at present that such a result simply reflects our limited ability to detect very low-temperature gas in starburst winds.

ACKNOWLEDGMENTS

We thank the referee for comments which improved the clarity of this paper. This work has made use of the 2 Micron All Sky Survey database, and the Lyon-Meudon (LEDA) and NASA/IPAC (NED) extragalactic databases. JR acknowledges support by the Danish Natural Science Research Council (SNF) and by the Instrument Center for Danish Astrophysics (IDA). TJP acknowledges the support of a Senior Fellowship from the Particle Physics and Astronomy Research Council.

REFERENCES

Anders E., Grevesse N., 1989, *Geochim. Cosmochim. Acta*, 53, 197
 Babul A., Rees M.J., 1992, *MNRAS*, 255, 346
 Benson A.J., Bower R.G., Frenk C.S., White S.D.M., 2000, *MNRAS*, 314, 557
 Birnboim Y., Dekel A., 2003, *MNRAS*, 345, 349
 Bomans D.J., Grant M.-B., 1998, *AN*, 319, 26
 Buote D.A., 2000, *MNRAS*, 311, 176
 Buote D.A., Lewis A.D., Brightenti F., Mathews W.G., 2003, *ApJ*, 595, 151
 Calzetti D., Bohlin R.C., Kinney A.L., Storchi-Bergmann T., Heckman T.M., 1995, *ApJ*, 443, 136
 Calzetti D., Harris J., Gallagher J.S., Smith D.A., Conselice C.J., Homeier N., Kewley L., 2004, *AJ*, 127, 1405
 Chevalier R.A., Clegg A.W., 1985, *Nature*, 317, 44
 Davis D.S., Mulchaey J.S., Mushotzky R.F., 1999, *ApJ*, 511, 34
 de Vaucouleurs G., de Vaucouleurs A., Corwin H.G., 1976, *The Second Reference Catalogue of bright galaxies (RC2)*, Univ. Texas Press, Austin, TX
 Devereux N.A., Eales S.A., 1989, *ApJ*, 340, 708
 Eke V.R., et al., 2004, *MNRAS*, 348, 866
 Evrard A.E., Henry J.P., 1991, *ApJ*, 383, 95
 Fabian A.C., Sanders J.S., Crawford C.S., Ettori S., 2003, *MNRAS*, 341, 729
 Fullmer L., Lonsdale C.J., 1989, *Catalogued galaxies and quasars observed in the IRAS survey. Version 2*.
 Gaetz T.J., Salpeter E.E., Shaviv G., 1987, *ApJ*, 316, 530
 Gallagher J.S., Hunter D.A., Knapp G.R., 1981, *AJ*, 86, 344
 Galliano F., Madden S.C., Jones A.P., Wilson C.D., Bernard J.-P., Le Peintre F., 2003, *A&A*, 407, 159
 Gehrels N., 1986, *ApJ*, 303, 336
 Hartwell J.M., Stevens I.R., Strickland D.K., Heckman T.M., Summers L.K., 2004, *MNRAS*, 348, 406
 Heckman T.M., 2003, in Avila-Reese V., Firmani C., Frenk C.S., Allen C., eds, *Rev. Mex. AA. Vol. 17, Galaxy Evolution: Theory & Observations*, p. 47
 Heckman T.M., Armus L., Miley G.K., 1990, *ApJS*, 74, 833
 Heckman T.M., Carmelle R., Leitherer C., Garnett D.R., van der Rydt F., 1998, *ApJ*, 503, 646
 Helsdon S.F., Ponman T.J., 2000, *MNRAS*, 315, 356
 Hunter D.A., 1996, *ApJ*, 457, 671
 Hunter D.A., van Woerden H., Gallagher J.S., 1994, *ApJS*, 91, 79
 Isobe T., Feigelson E.D., Akritas M.G., Babu G.J., 1990, *ApJ*, 364, 104

Kaiser N., 1991, *ApJ*, 383, 104

Kennicutt R.C., Jr., 1998, *ApJ*, 498, 541

Kennicutt R.C., Jr., Tamblyn P., Congdon C.E., 1994, *ApJ*, 435, 22

Koo B.-C., McKee C.F., 1992, *ApJ*, 388, 93

Larsen T.I., Sommer-Larsen J., Pagel B.E.J., 2001, *MNRAS*, 323, 555

Legrand F., Tenorio-Tagle G., Silich S., Kunth D., Cervino M., 2001, *ApJ*, 560, 630

Lehnert M.D., Heckman T.M., Weaver K.A., 1999, *ApJ*, 523, 575

Lisenfeld U., Ferrara A., 1998, *ApJ*, 496, 145

Mac Low M.-M., McCray R., 1988, *ApJ*, 324, 776

Mac Low M.-M., McCray R., Norman M.L., 1989, *ApJ*, 337, 141

Maia M.A.G., da Costa L.N., Latham D.W., 1989, *ApJS*, 69, 809

Marcolini A., Brighenti F., D'Ercole A., 2003, *MNRAS*, 345, 1329

Martin C.L., Kobulnicky H.A., Heckman T.M., 2002, *ApJ*, 574, 663

Mulchaey J.S., Davis D.S., Mushotzky R.F., Burstein D., 2003, *ApJS*, 145, 39

Murakami I., Babul A., 1999, *MNRAS*, 309, 161

Norman C.A., Ikeuchi S., 1989, *ApJ*, 345, 372

Ott J., Martin C.L., Walter F., 2003, *ApJ*, 594, 776

Ponman T.J., Cannon D.B., Navarro J.F., 1999, *Nature*, 397, 135

Ponman T.J., Sanderson A.J.R., Finoguenov A., 2003, *MNRAS*, 343, 331

Press W.H., Teukolsky S.A., Vetterling W.T., Flannery B.P., 1996, *Numerical Recipes in Fortran 77*, Cambridge Univ. Press, Cambridge, UK

Ptak A., Serlemitsos P., Yaqoob T., Mushotzky R., Tsuru T., 1997, *AJ*, 113, 1286

Rasmussen J., Ponman T.J., 2004, *MNRAS*, 349, 722

Read A.M., Ponman T.J., 1998, *MNRAS*, 297, 143

Read A.M., Ponman T.J., 2001, *MNRAS*, 328, 127 (RP01)

Read A.M., Ponman T.J., Strickland D.K., 1997, *MNRAS*, 286, 626

Sanders D.B., Mirabel I.F., 1996, *ARA&A*, 34, 749

Sanderson A.J.R., Ponman T.J., Finoguenov A., Lloyd-Davies E.J., Markevitch M., 2003, *MNRAS*, 340, 989

Silich S., Tenorio-Tagle G., 2001, *ApJ*, 552, 91

Spinoglio L., Andreani P., Malkan M.A., 2002, *ApJ*, 572, 105

Strickland D.K., Stevens I.R., 2000, *MNRAS*, 314, 511

Strickland D.K., Heckman T.M., Weaver K.A., Dahlem M., 2000, *AJ*, 120, 2965

Strickland D.K., Heckman T.M., Weaver K.A., Hoopes C.G., Dahlem M., 2002, *ApJ*, 568, 689

Strickland D.K., Heckman T.M., Colbert E.J.M., Hoopes C.G., Weaver K.A., 2004, *ApJS*, 151, 193

Summers L.K., Stevens I.R., Strickland D.K., Heckman T.M., 2003, *MNRAS*, 342, 690

Summers L.K., Stevens I.R., Strickland D.K., Heckman T.M., 2004, *MNRAS*, 351, 1

Sun M., Forman W., Vikhlinin A., Hornstrup A., Jones C., Murray S.S., 2003, *ApJ*, 598, 250

Thuan T.X., Bauer F.E., Papaderos P., Izotov Y.I., 2004, *ApJ*, 606, 213

Toft S., Rasmussen J., Sommer-Larsen J., Pedersen K., 2002, *MNRAS*, 335, 799

Tosi M., 2004, in STScI May Symposium, *The Local Group as an Astrophysical Laboratory*, Cambridge Univ. Press, Cambridge, in press (astro-ph/0308463)

Tully R.B., 1987, *ApJ*, 321, 280

Tully R.B., 1988, *Nearby Galaxies Catalog*, Cambridge Univ. Press, Cambridge

Turner M.J.L., et al., 2001, *A&A*, 365, L110

Wang B., 1995, *ApJ*, 444, 590

Wolfire M.G., McKee C.F., Hollenbach D., Tielens A.G.G.M., 1995, *ApJ*, 453, 673

Yun M.S., 1999, in Barnes J.E., Sanders D.B., eds, *Proc. IAU Symp. 186, Galaxy Interactions at Low and High Redshift*, Kluwer Academic Publishers, Dordrecht, p. 81

Zou Z-L., Xia X-Y., Deng Z-G., Wu H., 1995, *A&A*, 304, 369